

# Non-standard neutrino interactions in reactor and superbeam experiments

Joachim Kopp,<sup>a</sup> Manfred Lindner,<sup>b</sup> and Toshihiko Ota<sup>c</sup>

*Max-Planck-Institut für Kernphysik,  
Postfach 10 39 80, 69029 Heidelberg, Germany*

Joe Sato<sup>d</sup>

*Department of Physics, Saitama University, Shimo-Okubo 255,  
Sakura-ku, Saitama, 338-8570, Japan*

The formalism of non-standard four-fermion interactions provides a convenient, model-independent way of parameterizing a wide class of “new physics” scenarios. In this article, we study the performance of reactor and superbeam neutrino experiments in the presence of such non-standard interactions (NSI). Due to interference between the standard and non-standard amplitudes, sizeable effects are to be expected if the NSI parameters are close to their current upper limits. We derive approximate formulas for the relevant oscillation probabilities including NSI, and show how the leading effects can be understood intuitively even without any calculations. We will present a classification of all possible NSI according to their impact on reactor and superbeam experiments, and it will turn out that these experiments are highly complementary in terms of their sensitivity to the non-standard parameters. The second part of the paper is devoted to detailed numerical simulations, which will demonstrate how a standard oscillation fit of the mixing angle  $\theta_{13}$  may fail if experimental data is affected by NSI. We find that for some non-standard terms, reactor and superbeam experiments would yield seemingly conflicting results, while in other cases, they may agree well with each other, but the resulting value for  $\theta_{13}$  could be far from the true value. This offset may be so large that the true  $\theta_{13}$  is even ruled out erroneously. In the last section of the paper, we demonstrate that reactor and superbeam data can actually establish the presence of non-standard interactions. Throughout our discussion, we pay special attention to the impact of the complex phases, and of the near detectors.

PACS numbers: 13.15.+g, 14.60.Pq, 12.60.-i

Keywords: neutrino oscillations, non-standard interactions, reactor experiments, superbeams

## 1. INTRODUCTION

At the dawn of the era beyond the standard model, a plethora of new theoretical models has been devised to resolve many of the experimental and theoretical shortcomings of our current picture of elementary particles. However, in the context of future experiments, it is often desirable to describe new physics in a more model-independent way. One possibility to achieve this is through effective four-fermion operators, so-called non-standard interactions (NSI), which arise naturally in the presence of heavy mediator fields. In this article, we shall focus in particular on NSI in the neutrino sector, which have been discussed on general phenomenological grounds in [1, 2, 3, 4, 5, 6, 7, 8], and in the context of specific models in [9, 10, 11, 12]. The importance of NSI for neutrino oscillation physics

has been pointed out in a pioneering work by Grossman [13], and many authors have studied their impact on solar neutrinos [14, 15, 16, 17], atmospheric neutrinos [18, 19, 20, 21, 22, 23], conventional and upgraded neutrino beams [24, 25, 26, 27, 28, 29, 30], neutrino factories [8, 25, 31, 32, 33, 34, 35, 36, 37], beta beams [38], supernova neutrinos [39, 40, 41], cosmological relic neutrinos [42],  $e^+e^-$  colliders [43], neutrino-electron scattering [44], and neutrino-nucleus scattering [45, 46]. Existing experimental bounds are presented in [47].

Our main interest in this work will be on non-standard interactions in upcoming reactor and accelerator neutrino experiments. Although the main design goal for these experiments is the precision measurement of the standard oscillation parameters, the search for deviations from the standard framework is an equally interesting part of their physics program. Moreover, while in the race for the standard oscillation parameters, reactor and beam experiments are competing, we will show that their results will be highly complementary when one is interested in non-standard physics.

In the numerical simulations which we are going to present, we will focus on the experiments T2K [48, 49],

<sup>a</sup>Email: jkopp@mpi-hd.mpg.de

<sup>b</sup>Email: lindner@mpi-hd.mpg.de

<sup>c</sup>Email: toshi@mpi-hd.mpg.de

<sup>d</sup>Email: joe@phy.saitama-u.ac.jp

NO $\nu$ A [50], Double Chooz [51, 52], and a hypothetical 200 t reactor experiment [53]. Of course, the analytical results apply also to other experiments such as T2HK [48] and Daya Bay [54].

We will first introduce our formalism in Sec. 2, and give a detailed discussion of the different possible Lorentz structures and their relevance for reactor and superbeam experiments. Although this discussion may seem rather technical, it will ultimately allow us to greatly simplify the problem and considerably reduce the number of parameters. In Sec. 3, we will then present approximate expressions for the oscillation probabilities including NSI for the  $\bar{\nu}_e \rightarrow \bar{\nu}_e$ ,  $\nu_\mu \rightarrow \nu_e$ , and  $\nu_\mu \rightarrow \nu_\mu$  channels. We will also show in an intuitive way why certain NSI terms appear in these expressions, and others do not. Sec. 4 is devoted to a discussion of numerical simulation techniques, and of the specific experiments which we have simulated. In Sec. 5, we show how the data from these experiments may be misinterpreted, if NSI are not taken into account in the fits. We will finally demonstrate in Sec. 6, that a combined analysis of reactor and superbeam data may allow for the actual discovery of a wide variety of non-standard interactions by goodness-of-fit arguments. Our conclusions will be presented in Sec. 7.

## 2. THE FORMALISM OF NON-STANDARD INTERACTIONS

### 2.1. The NSI Lagrangian

It is well known that in the low energy regime, weak neutrino interactions can be described by effective four-fermion operators like

$$\mathcal{L}_\nu = \frac{G_F}{\sqrt{2}} [\bar{\nu}_\alpha \gamma^\rho (1 - \gamma^5) \ell_\alpha] [\bar{f}' \gamma_\rho (1 - \gamma^5) f], \quad (1)$$

and

$$\mathcal{L}_{\text{MSW}} = \frac{G_F}{\sqrt{2}} [\bar{\nu}_\alpha \gamma^\rho (1 - \gamma^5) \nu_\alpha] [\bar{f}' \gamma_\rho (1 - \gamma^5) f], \quad (2)$$

where  $\nu_\alpha$  is the neutrino field of flavor  $\alpha$ ,  $\ell_\alpha$  is the corresponding charged lepton field, and  $f, f'$  are the components of an arbitrary weak doublet.

The low-energy fingerprint of many “new physics” scenarios has a structure similar to Eqs. (1) and (2), and the corresponding operators are called non-standard interactions. If we consider only lepton number conserving operators, the most general NSI Lagrangian reads

$$\mathcal{L}_{\text{NSI}} = \mathcal{L}_{V\pm A} + \mathcal{L}_{S\pm P} + \mathcal{L}_T, \quad (3)$$

where the different terms are classified according to their Lorentz structure in the following way:

$$\mathcal{L}_{V\pm A} =$$

$$\begin{aligned} & \frac{G_F}{\sqrt{2}} \sum_{f,f'} \tilde{\varepsilon}_{\alpha\beta}^{s,f,f',V\pm A} [\bar{\nu}_\beta \gamma^\rho (1 - \gamma^5) \ell_\alpha] [\bar{f}' \gamma_\rho (1 \pm \gamma^5) f] + \\ & \frac{G_F}{\sqrt{2}} \sum_f \tilde{\varepsilon}_{\alpha\beta}^{m,f,V\pm A} [\bar{\nu}_\alpha \gamma^\rho (1 - \gamma^5) \nu_\beta] [\bar{f}' \gamma_\rho (1 \pm \gamma^5) f] + \text{h.c.}, \end{aligned} \quad (4)$$

$$\mathcal{L}_{S\pm P} = \frac{G_F}{\sqrt{2}} \sum_{f,f'} \tilde{\varepsilon}_{\alpha\beta}^{s,f,f',S\pm P} [\bar{\nu}_\beta (1 + \gamma^5) \ell_\alpha] [\bar{f}' (1 \pm \gamma^5) f], \quad (5)$$

$$\mathcal{L}_T = \frac{G_F}{\sqrt{2}} \sum_{f,f'} \tilde{\varepsilon}_{\alpha\beta}^{s,f,f',T} [\bar{\nu}_\beta \sigma^{\rho\tau} \ell_\alpha] [\bar{f}' \sigma_{\rho\tau} f]. \quad (6)$$

Here,  $G_F$ , is the Fermi constant,  $\nu$  and  $\ell$  are the neutrino and charged lepton fields, and the  $f$ 's represent the interaction partners of the neutrinos. The dimensionless parameters  $\tilde{\varepsilon}$  give the strength of the non-standard interactions relative to  $G_F$ , where an upper index  $s$  stands for NSI in the neutrino source or detector, while  $m$  denotes non-standard matter effects, i.e. NSI affecting the propagation. In general, the  $\tilde{\varepsilon}^s$  can be arbitrary complex matrices, while the  $\tilde{\varepsilon}^m$  have to be hermitian.

Note that we have required the neutrino fields to be purely left-handed, since processes involving right handed neutrinos would require either a neutrino helicity flip, or their amplitudes would have to contain at least two NSI terms (e.g. one to create the right-handed neutrino and one to absorb it), and would therefore be strongly suppressed. This constraint on the neutrino chirality in particular forbids  $\nu\nu f f$  terms in  $\mathcal{L}_{S\pm P}$  and  $\mathcal{L}_T$ .

Before proceeding, let us give a simple estimate which relates the magnitude of the  $\tilde{\varepsilon}$  parameters to the corresponding new physics scale  $M_{\text{NSI}}$  [31]: If we assume the non-standard interactions to be mediated by some intermediate particles with a mass of order  $M_{\text{NSI}}$ , the effective vertices in Eqs. (4) – (6) will be suppressed by  $1/M_{\text{NSI}}^2$  in the same way as the standard weak interactions are suppressed by  $1/M_{\text{W}}^2$ . Therefore we expect

$$|\tilde{\varepsilon}| \sim \frac{M_{\text{W}}^2}{M_{\text{NSI}}^2}. \quad (7)$$

### 2.2. Relevance of the different NSI terms to reactor and superbeam experiments

We see from Eqs. (4) – (6) that the number of possible NSI terms is very large. However, the number of parameters for our discussion of reactor and superbeam experiments can be greatly reduced by a few simple, but rather technical arguments. Many of these arguments are based on constraints coming from the requirement of interference between the standard and non-standard amplitudes. Of course, the total interaction rate will also contain pure NSI terms, for which these constraints do not apply; but they are suppressed by  $\tilde{\varepsilon}^2$ , and can therefore be assumed to be negligible compared to the

interference terms, which are linear in  $\tilde{\varepsilon}$ . The following arguments are also summarized in Tab. I.

1. The standard production and detection processes of reactor and superbeam neutrinos are, on the fundamental level, decays of  $u$  quarks into  $d$  quarks, or vice-versa. Since interference of standard and non-standard amplitudes requires the external particles to be identical, only the  $\tilde{\varepsilon}^{s,f,f'}$  terms with  $f = u$ ,  $f' = d$  will be relevant, and we will henceforth simply omit the indices  $f$  and  $f'$ .
2. For the non-standard matter effects, only coupling to electrons, up quarks, and down quarks is important.
3. Non-standard couplings involving  $\tau$  leptons are irrelevant since  $\tau$  production is impossible in reactor and beam sources, and is not considered as a detection process here, although it might in principle be possible for high energy superbeam neutrinos. Hence we take

$$\tilde{\varepsilon}_{\tau\beta}^{s,V\pm A} = \tilde{\varepsilon}_{\tau\beta}^{s,S\pm P} = \tilde{\varepsilon}_{\tau\beta}^{s,T} = 0 \quad (8)$$

For the same reason, processes involving muons can be neglected in reactor experiments, and processes involving electrons can be neglected in the superbeam source, since they constitute subdominant backgrounds even in the standard framework.

4. In the couplings to muons, there is still room for non- $(V - A)(V - A)$  contributions. For neutrino production in pion decay, the effect of  $(S + P)(S \pm P)$  type NSI is even enhanced by a factor of [55, 56]

$$\omega = \frac{m_\pi}{m_\mu} \frac{m_\pi}{m_u + m_d} \sim 20, \quad (9)$$

and the importance of this enhancement for accelerator neutrino experiments has been pointed out in [26]. However, there exist limits on the muon helicity in pion decay [57, 58], which ensure that, in spite of the enhancement,  $(S + P)(S \pm P)$  type NSI cannot affect the neutrino oscillation amplitude by more than a few per cent.

5. Tensor interactions are impossible in pion decay since the decay operator must have a parity-odd component.
6. In the detection processes involving muons, the  $(S + P)(S \pm P)$  and  $TT$  terms are chirally suppressed by the smallness of  $m_\mu$  compared to the typical superbeam energies of  $\mathcal{O}(1 \text{ GeV})$ . As mentioned above, the leading effect in the total event rate is given by the interference of the non-standard amplitude and the standard  $(V - A)(V - A)$  amplitude. This interference can only occur if the initial and final state particles have identical helicities,

so for  $(S + P)(S \pm P)$  and  $TT$  type non-standard interactions, a mass-suppressed helicity flip of the muon is required. We can also see the emergence of the suppression factor explicitly by considering the Dirac traces, which have to be evaluated when calculating the cross section. For example, in the case of  $(S + P)(S + P)$  NSI, the spin sum in the interference term of standard and non-standard amplitudes is

$$\begin{aligned} & \sum_{\text{spins}} \text{Tr}[\gamma^\rho(1 - \gamma^5)\mu\bar{\mu}(1 - \gamma^5)\nu\bar{\nu}] \\ & \cdot \text{Tr}[\gamma_\rho(1 - \gamma^5)u\bar{u}(1 - \gamma^5)d\bar{d}] \\ = & \sum_{\text{spins}} \text{Tr}[\gamma^\rho(1 - \gamma^5)(\not{p}_\mu + m_\mu)(1 - \gamma^5)(\not{p}_\nu + m_\nu)] \\ & \cdot \text{Tr}[\gamma_\rho(1 - \gamma^5)(\not{p}_u + m_u)(1 - \gamma^5)(\not{p}_d + m_d)]. \end{aligned} \quad (10)$$

Similar equations can be derived for  $(S + P)(S - P)$  and  $TT$  interactions. Due to the orthogonality property of the chirality projection operators, a contribution proportional to  $m_\mu$  remains of the first trace in Eq. (10), and a contribution proportional to  $m_u$  from the second. This leads to a suppression factor of  $\mathcal{O}(m_\mu m_u/E^2)$ . Low energy neutrinos ( $E \lesssim 1 \text{ GeV}$ ) interact with whole nucleons, rather than single quarks, therefore  $m_u$  should be replaced by the much larger nucleon mass  $m_n$ , so that in this case, the overall chiral suppression is only of  $\mathcal{O}(m_\mu/E)$ . At typical superbeam energies around 1 GeV, we are in the transition regime between neutrino-nucleon interactions (quasielastic scattering and resonance scattering) and neutrino-quark interactions (deep-inelastic scattering) [59, 60].

7. For  $(V - A)(V + A)$  interactions involving muons in the detector, chiral suppression occurs only for the hadronic interaction partners, and according to our above discussion, it is not very pronounced for them. Therefore,  $(V - A)(V + A)$  type interactions may in general be important for the cross sections, and modify their overall magnitude as well as their energy dependence.
8. From measurements of the electron angular distribution in nuclear  $\beta$  decays,  $(S + P)(S \pm P)$  and  $TT$  couplings to electrons are strongly constrained [61, 62, 63, 64, 65]. Consequently, we take

$$\tilde{\varepsilon}_{e\beta}^{s,S\pm P} = \tilde{\varepsilon}_{e\beta}^{s,T} = 0 \quad (11)$$

for  $\beta = e, \mu, \tau$ .

9. There is still room for  $(V - A)(V + A)$  type terms involving electrons, because these terms differ from the standard model term only in the quark current, which cannot be directly measured. Limits exist only for the effective vector and axial-vector couplings of protons and neutrons [65], but due to the

**Reactor source and detector ( $f = u, f' = d$ )**

	Source			Detector		
	$l_\alpha = e$	$l_\alpha = \mu$	$l_\alpha = \tau$	$l_\alpha = e$	$l_\alpha = \mu$	$l_\alpha = \tau$
$V - A$	✓	no $\mu$ production	no $\tau$ production	✓	no $\mu$ production	no $\tau$ production
$V + A$	✓	no $\mu$ production	no $\tau$ production	✓	no $\mu$ production	no $\tau$ production
$S - P$	strong constraints	no $\mu$ production	no $\tau$ production	strong constraints	no $\mu$ production	no $\tau$ production
$S + P$	strong constraints	no $\mu$ production	no $\tau$ production	strong constraints	no $\mu$ production	no $\tau$ production
$T$	strong constraints	no $\mu$ production	no $\tau$ production	strong constraints	no $\mu$ production	no $\tau$ production

**Superbeam source and detector ( $f = u, f' = d$ )**

	Source			Detector		
	$l_\alpha = e$	$l_\alpha = \mu$	$l_\alpha = \tau$	$l_\alpha = e$	$l_\alpha = \mu$	$l_\alpha = \tau$
$V - A$	no $e$ production	✓	no $\tau$ production	✓	✓	no $\tau$ detection
$V + A$	no $e$ production	✓	no $\tau$ production	✓ (mild supp.)	✓ (mild supp.)	no $\tau$ detection
$S - P$	no $e$ production	✓	no $\tau$ production	strong constraints	chiral supp.	no $\tau$ detection
$S + P$	no $e$ production	✓	no $\tau$ production	strong constraints	chiral supp.	no $\tau$ detection
$T$	no $e$ production	no $P$ -odd part	no $\tau$ production	strong constraints	chiral supp.	no $\tau$ detection

**Propagation ( $f = e, u, d$ )**

$V - A$	✓
$V + A$	✓

Table I: Classification of the vertices from Eqs. (4) – (6) according to their impact on reactor and superbeam experiments. Terms marked with ✓ can give a sizeable contribution; for all other terms, the reason for their suppression is given (see text for details).

non-perturbative nature of the strong interactions, these cannot be easily related to the couplings of the fundamental quarks.

If  $(V - A)(V + A)$  couplings to electrons exist, the processes in which they appear will in general have an energy dependence different from that of the corresponding standard processes. For anti-neutrino production in nuclear reactors, however, this difference is completely negligible because the neutrino spectrum from nuclear  $\beta$  decay is governed by kinematical effects and by the Fermi function, which describes final state Coulomb interactions.

The cross section for the inverse  $\beta$  decay process, which is used to detect reactor anti-neutrinos, is derived from empirical values for the effective vector and axial-vector couplings, so any possible  $(V - A)(V + A)$  contribution is automatically taken into account properly.

Finally,  $(V - A)(V + A)$  interactions involving electrons in the beam detector, are mildly chirally suppressed, in analogy to  $(V - A)(V + A)$  interactions involving muons.

10. As we have seen in Eqs. (4) – (6), non-standard matter effects can only have a  $(V - A)(V - A)$

or  $(V - A)(V + A)$  Lorentz structure, as long as we restrict the discussion to left-handed neutrinos. For the computation of the coherent forward scattering amplitude, the factor  $[\bar{f}\gamma_\rho(1 \pm \gamma^5)f]$  has to be averaged over the neutrino trajectory, and for unpolarized matter at rest, the only contribution is  $N_f = \bar{f}\gamma^0 f$ , the fermion density appearing in the matter potential. Since  $N_f$  is independent of the axial current, we conclude that both possible Lorentz structures would have the same impact on the non-standard matter effects.

To conclude this discussion, we would like to emphasize again that non- $(V - A)(V - A)$  Lorentz structures can play an important role in reactor and superbeam experiments. However, these experiments do not have the capability to distinguish different Lorentz structures, unless the spectral distortion caused by  $(V - A)(V + A)$  terms in the superbeam detector is taken into account. In the following, we will neglect this spectral distortion for simplicity, assuming that it is anyway hidden by the systematical uncertainties in the neutrino cross sections.

### 2.3. Hamiltonian approach to non-standard interactions in neutrino oscillations

The observations from the previous section can be exploited to further reduce the number of free parameters in our problem. To this end, we define effective couplings  $\varepsilon_{\alpha\beta}^s$ ,  $\varepsilon_{\alpha\beta}^d$ , and  $\varepsilon_{\alpha\beta}^m$ , corresponding to non-standard interactions in the production, detection, and propagation processes.  $\varepsilon_{\alpha\beta}^s$  describes a non-standard admixture of flavor  $\beta$  to the neutrino state which is produced in association with a charged lepton of flavor  $\alpha$ . This means, that the neutrino source does not produce a pure flavor neutrino eigenstate  $|\nu_\alpha\rangle$ , but rather a state

$$|\nu_\alpha^s\rangle = |\nu_\alpha\rangle + \sum_{\beta=e,\mu,\tau} \varepsilon_{\alpha\beta}^s |\nu_\beta\rangle. \quad (12)$$

Similarly, the detector is sensitive not to the normal weak eigenstates, but to the combination

$$\langle\nu_\beta^d| = \langle\nu_\beta| + \sum_{\alpha=e,\mu,\tau} \varepsilon_{\alpha\beta}^d \langle\nu_\alpha|. \quad (13)$$

Note that in  $\varepsilon_{\alpha\beta}^s$ , the first index corresponds to the flavor of the charged lepton, and the second to that of the neutrino, while in  $\varepsilon_{\alpha\beta}^d$ , the order is reversed. We have chosen this convention to be consistent with the literature.

In general, the matrices  $(1 + \varepsilon^s)$  and  $(1 + \varepsilon^d)$  are non-unitary, i.e. the source and detection states are not required to form complete orthonormal sets of basis vectors in the Hilbert space:

$$\sum_{\alpha=e,\mu,\tau} |\nu_\alpha^s\rangle\langle\nu_\alpha^s| \neq 1, \quad \sum_{\beta=e,\mu,\tau} |\nu_\beta^d\rangle\langle\nu_\beta^d| \neq 1, \quad (14)$$

$$\langle\nu_\alpha^s|\nu_\beta^s\rangle \neq \delta_{\alpha\beta} \quad \langle\nu_\alpha^d|\nu_\beta^d\rangle \neq \delta_{\alpha\beta}. \quad (15)$$

We can read off from Tab. I that the  $3 \times 3$  coupling matrix  $\varepsilon_{\alpha\beta}^s$  receives contributions from  $\tilde{\varepsilon}_{\alpha\beta}^{s,u,d,V\pm A}$  and  $\tilde{\varepsilon}_{\alpha\beta}^{s,u,d,S\pm P}$ , while  $\varepsilon_{\alpha\beta}^d$  and  $\varepsilon_{\alpha\beta}^m$  are built up only from  $(V - A)(V \pm A)$  contributions.

Since the coefficients  $\varepsilon_{e\alpha}^s$  and  $\varepsilon_{\alpha e}^d$  (for  $\alpha = e, \mu, \tau$ ) both originate from  $\tilde{\varepsilon}^{s,u,d,V\pm A}$ , the  $(V - A)(V \pm A)$  coupling to up and down quarks, we have the constraint

$$\varepsilon_{e\alpha}^s = \varepsilon_{\alpha e}^{d*}, \quad (16)$$

which again reduces the number of independent parameters by 3. The aforementioned spectral distortion and

mild chiral suppression in the superbeam detector could invalidate Eq. (16), but we will neglect it in the following.

Similarly, the  $(V - A)(V \pm A)$  part of  $\varepsilon_{\mu\alpha}^s$  and  $\varepsilon_{\alpha\mu}^d$  are the same, and since the  $(S + P)(S \pm P)$  Lorentz structures have less impact in  $\varepsilon_{\alpha\mu}^d$  than in  $\varepsilon_{\mu\alpha}^s$ , we will typically have

$$|\varepsilon_{\mu\alpha}^s| \gtrsim |\varepsilon_{\alpha\mu}^d| \quad (17)$$

(barring fine-tuned cancellation effects). If we assume all non-standard interactions to be of the  $(V - A)(V - A)$  type, as is sometimes done in the literature, the constraints from Eqs. (16) and (17) are tightened to  $\varepsilon^s = (\varepsilon^d)^\dagger$ .

It is clear from Tab. I that coupling to  $\tau$  leptons is irrelevant in our case, so we can also take

$$\varepsilon_{\tau\beta}^s = \varepsilon_{\alpha\tau}^d = 0 \quad (18)$$

for all  $\alpha, \beta$ .

$\varepsilon^m$  is an additive contribution to the Mikheyev-Smirnov-Wolfenstein (MSW) potential in the flavor basis,  $V_{\text{MSW}} = a_{\text{CC}} \text{diag}(1, 0, 0)$ , which now becomes

$$\tilde{V}_{\text{MSW}} = a_{\text{CC}} \begin{pmatrix} 1 + \varepsilon_{ee}^m & \varepsilon_{e\mu}^m & \varepsilon_{e\tau}^m \\ \varepsilon_{e\mu}^{m*} & \varepsilon_{\mu\mu}^m & \varepsilon_{\mu\tau}^m \\ \varepsilon_{e\tau}^{m*} & \varepsilon_{\mu\tau}^{m*} & \varepsilon_{\tau\tau}^m \end{pmatrix}, \quad (19)$$

with  $a_{\text{CC}} = 2\sqrt{2}G_F N_e E$ . Recall from Eq. (4) that the diagonal entries in this matrix have to be real, so that the Hamiltonian will remain hermitian, and can be diagonalized by a unitary mixing matrix.

Since we are interested in a combined analysis of reactor and superbeam experiments, it is important to keep in mind that the effective  $\varepsilon$  matrices are *the same* for both types of experiments, because, under the assumptions and approximations discussed above, those entries which may be relevant in both of them ( $\varepsilon_{\alpha\beta}^m$  and  $\varepsilon_{\alpha e}^d$ ) are identical in both cases.

The oscillation probability is obtained as

$$\begin{aligned} P_{\nu_\alpha^s \rightarrow \nu_\beta^d} &= |\langle\nu_\beta^d|e^{-iHL}|\nu_\alpha^s\rangle|^2 \\ &= |(1 + \varepsilon^d)_{\gamma\beta} (e^{-iHL})_{\gamma\delta} (1 + \varepsilon^s)_{\alpha\delta}|^2 \\ &= \left| \left[ (1 + \varepsilon^d)^T e^{-iHL} (1 + \varepsilon^s)^T \right]_{\beta\alpha} \right|^2, \quad (20) \end{aligned}$$

where

$$H_{\alpha\beta} = \frac{1}{2E} \left[ U_{\alpha j} \begin{pmatrix} 0 & & \\ & \Delta m_{21}^2 & \\ & & \Delta m_{31}^2 \end{pmatrix}_{jk} (U^\dagger)_{k\beta} + (\tilde{V}_{\text{MSW}})_{\alpha\beta} \right]. \quad (21)$$

The Pontecorvo-Maki-Nakagawa-Sakata (PMNS) matrix  $U$  is parameterized as

$$U = \begin{pmatrix} c_{12}c_{13} & s_{12}c_{13} & s_{13}e^{-i\delta_{\text{CP}}} \\ -s_{12}c_{23} - c_{12}s_{13}s_{23}e^{i\delta_{\text{CP}}} & c_{12}c_{23} - s_{12}s_{13}s_{23}e^{i\delta_{\text{CP}}} & c_{13}s_{23} \\ s_{12}s_{23} - c_{12}s_{13}c_{23}e^{i\delta_{\text{CP}}} & -c_{12}s_{23} - s_{12}s_{13}c_{23}e^{i\delta_{\text{CP}}} & c_{13}c_{23} \end{pmatrix}. \quad (22)$$

As usual,  $s_{ij}$  and  $c_{ij}$  denote the sine and cosine of the mixing angle  $\theta_{ij}$ , and  $\delta_{\text{CP}}$  is the (Dirac) CP phase.

For anti-neutrinos, we have to replace  $\varepsilon^s$ ,  $\varepsilon^d$ , and  $\varepsilon^m$  by their complex conjugates in the above equations, and reverse the signs of  $a_{\text{CC}}$  and  $\delta_{\text{CP}}$ .

#### 2.4. Perturbative calculation of oscillation probabilities

In practice, it is very convenient to expand the oscillation probabilities in a perturbative series with respect to the small quantities  $\theta_{13}$ ,  $\Delta m_{21}^2/\Delta m_{31}^2$ , and  $|\varepsilon_{\alpha\beta}^{s,m,d}|$  instead of attempting to evaluate Eq. (20) exactly. Following a procedure similar to the one explained in the appendix of [66], the first order expansion reads

$$P_{\nu_\alpha^s \rightarrow \nu_\beta^d} = P_{\nu_\alpha^s \rightarrow \nu_\beta^d}^{(0)} + P_{\nu_\alpha^s \rightarrow \nu_\beta^d}^{(1)} + \dots, \quad (23)$$

where

$$\begin{aligned} P_{\nu_\alpha^s \rightarrow \nu_\beta^d}^{(0)} &= \left| \left[ e^{-iH^{(0)}L} \right]_{\beta\alpha} \right|^2, \\ P_{\nu_\alpha^s \rightarrow \nu_\beta^d}^{(1)} &= \left[ e^{-iH^{(0)}L} \right]_{\beta\alpha}^* \left[ e^{-iH^{(0)}L} (1 + \varepsilon^s)^T \right]_{\beta\alpha} \\ &\quad + \left[ e^{-iH^{(0)}L} \right]_{\beta\alpha}^* \left[ (1 + \varepsilon^d)^T e^{-iH^{(0)}L} \right]_{\beta\alpha} \\ &\quad - i \left[ e^{-iH^{(0)}L} \right]_{\beta\alpha}^* \left[ \int_0^L dx e^{-iH^{(0)}(L-x)} H^{(1)} e^{-iH^{(0)}x} \right]_{\beta\alpha} \\ &\quad + \text{h.c.}, \end{aligned} \quad (24)$$

and

$$\begin{aligned} H_{\alpha\beta}^{(0)} &= \frac{1}{2E} \left[ U^{(0)} \begin{pmatrix} 0 & & \\ & 0 & \\ & & \Delta m_{31}^2 \end{pmatrix} U^{(0)\dagger} \right. \\ &\quad \left. + a_{\text{CC}} \begin{pmatrix} 1 & & \\ & 0 & \\ & & 0 \end{pmatrix} \right], \\ H_{\alpha\beta}^{(1)} &= \frac{1}{2E} \left[ U^{(0)} \begin{pmatrix} 0 & & \\ & \Delta m_{21}^2 & \\ & & 0 \end{pmatrix} U^{(0)\dagger} \right. \\ &\quad \left. + U^{(1)} \begin{pmatrix} 0 & & \\ & 0 & \\ & & \Delta m_{31}^2 \end{pmatrix} U^{(0)\dagger} \right], \end{aligned} \quad (26)$$

$$\begin{aligned} &+ U^{(0)} \begin{pmatrix} 0 & & \\ & 0 & \\ & & \Delta m_{31}^2 \end{pmatrix} U^{(1)\dagger} \\ &+ a_{\text{CC}} \begin{pmatrix} \varepsilon_{ee}^m & \varepsilon_{e\mu}^m & \varepsilon_{e\tau}^m \\ \varepsilon_{e\mu}^{m*} & \varepsilon_{\mu\mu}^m & \varepsilon_{\mu\tau}^m \\ \varepsilon_{e\tau}^{m*} & \varepsilon_{\mu\tau}^{m*} & \varepsilon_{\tau\tau}^m \end{pmatrix} \end{aligned} \quad (27)$$

By  $U^{(0)}$ , we denote the PMNS matrix for  $\theta_{13} = 0$ , and  $U^{(1)}$  contains the first order terms in  $\theta_{13}$ . The unperturbed Hamiltonian,  $H_{\alpha\beta}^{(0)}$ , can be easily diagonalized exactly, so that the matrix exponentials in the above equations can be evaluated. It is straightforward to extend the expansion to higher orders.

### 3. MODIFIED NEUTRINO OSCILLATION PROBABILITIES FOR REACTOR AND SUPERBEAM EXPERIMENTS

To study the impact of non-standard interactions on reactor and superbeam experiments, we need in particular the oscillation probabilities  $P_{\bar{\nu}_e^s \rightarrow \bar{\nu}_e^d}$ ,  $P_{\nu_\mu^s \rightarrow \nu_e^d}$ , and  $P_{\nu_\mu^s \rightarrow \nu_\mu^d}$ , to which these experiments are sensitive. We will first present approximate analytic formulas for these quantities in Secs. 3.1 to 3.3, and then discuss them in Sec. 3.4. All approximations were carried out with the perturbative method described in the previous section. We have checked that the expressions presented in this section reduce to the well-known standard oscillation results if NSI are absent by comparing them to the expressions derived in [66, 67, 68]. Moreover, we have verified all formulas numerically, term by term, using Mathematica.

To simplify the notation, let us make the abbreviations  $s_{ij} = \sin \theta_{ij}$ ,  $c_{ij} = \cos \theta_{ij}$ ,  $s_{2 \times ij} = \sin 2\theta_{ij}$ , and  $c_{2 \times ij} = \cos 2\theta_{ij}$ . Moreover, it will be convenient to split the  $\varepsilon$  parameters into their real and imaginary parts by writing  $\varepsilon_{\alpha\beta}^{s,m,d} = |\varepsilon_{\alpha\beta}^{s,m,d}| \exp(i\phi_{\alpha\beta}^{s,m,d})$ . To keep our results as general as possible, we will *not* impose the constraint from Eq. (16), but treat  $\varepsilon^s$  and  $\varepsilon^d$  as completely independent matrices. Thus, our formulas will be also applicable to experiments with fundamentally different production and detection processes, e.g. to a neutrino factory, where the production occurs through a purely leptonic  $\nu\nu e\mu$  vertex, while the detection process  $\nu l u d$  involves coupling to quarks. For reactors and superbeams, it is, of course, straightforward to impose Eq. (16) a posteriori.

### 3.1. The $\bar{\nu}_e \rightarrow \bar{\nu}_e$ channel

In a reactor experiment, the ratio  $L/E$  is chosen close to the first atmospheric oscillation maximum, so we can safely neglect terms proportional to  $\Delta m_{21}^2/\Delta m_{31}^2$ . Moreover, matter effects are irrelevant, i.e. we can take  $a_{CC} = 0$ . Finally, we will neglect terms suppressed by  $s_{13}^3$ ,  $\varepsilon s_{13}^2$ , or  $\varepsilon^2$ . The last approximation implies that we only consider the interference terms between standard and non-standard contributions, but not the pure, incoherent, NSI effect. This is justified for most realistic extensions of the Standard Model, where  $\varepsilon \ll 1$ , but it has been pointed out in [28] that, from current model-independent experimental limits, the NSI might even dominate over the standard oscillations in some situations. We find for the oscillation probability

$$\begin{aligned}
P_{\bar{\nu}_e^s \rightarrow \bar{\nu}_e^d} &= 1 - 4s_{13}^2 \sin^2 \frac{\Delta m_{31}^2 L}{4E} \\
&+ 2|\varepsilon_{ee}^s| \cos \phi_{ee}^s + 2|\varepsilon_{ee}^d| \cos \phi_{ee}^d \\
&- 4|\varepsilon_{e\mu}^s| s_{13} s_{23} \cos(\delta_{\text{CP}} - \phi_{e\mu}^s) \sin^2 \frac{\Delta m_{31}^2 L}{4E} \\
&+ 2|\varepsilon_{e\mu}^s| s_{13} s_{23} \sin(\delta_{\text{CP}} - \phi_{e\mu}^s) \sin \frac{\Delta m_{31}^2 L}{2E} \\
&- 4|\varepsilon_{e\tau}^s| s_{13} c_{23} \cos(\delta_{\text{CP}} - \phi_{e\tau}^s) \sin^2 \frac{\Delta m_{31}^2 L}{4E} \\
&+ 2|\varepsilon_{e\tau}^s| s_{13} c_{23} \sin(\delta_{\text{CP}} - \phi_{e\tau}^s) \sin \frac{\Delta m_{31}^2 L}{2E} \\
&- 4|\varepsilon_{\mu e}^d| s_{13} s_{23} \cos(\delta_{\text{CP}} + \phi_{\mu e}^d) \sin^2 \frac{\Delta m_{31}^2 L}{4E} \\
&- 2|\varepsilon_{\mu e}^d| s_{13} s_{23} \sin(\delta_{\text{CP}} + \phi_{\mu e}^d) \sin \frac{\Delta m_{31}^2 L}{2E} \\
&- 4|\varepsilon_{\tau e}^d| s_{13} c_{23} \cos(\delta_{\text{CP}} + \phi_{\tau e}^d) \sin^2 \frac{\Delta m_{31}^2 L}{4E} \\
&- 2|\varepsilon_{\tau e}^d| s_{13} c_{23} \sin(\delta_{\text{CP}} + \phi_{\tau e}^d) \sin \frac{\Delta m_{31}^2 L}{2E} \\
&+ \mathcal{O}\left(\frac{\Delta m_{21}^2}{\Delta m_{31}^2}\right) + \mathcal{O}(\varepsilon s_{13}^2) + \mathcal{O}(s_{13}^3) + \mathcal{O}(\varepsilon^2).
\end{aligned} \tag{28}$$

It is interesting to remark that, due to the  $\varepsilon_{ee}^s$  and  $\varepsilon_{ee}^d$  terms, this expression can be different from unity even for  $\Delta m_{31}^2 L/4E \ll 1$ , i.e. at the near detector (ND) site. Indeed, we obtain in this case

$$\begin{aligned}
P_{\bar{\nu}_e^s \rightarrow \bar{\nu}_e^d}^{\text{ND}} &= 1 + 2|\varepsilon_{ee}^s| \cos \phi_{ee}^s + 2|\varepsilon_{ee}^d| \cos \phi_{ee}^d + |\varepsilon_{ee}^s|^2 + |\varepsilon_{ee}^d|^2 \\
&+ 2|\varepsilon_{ee}^s| |\varepsilon_{ee}^d| [\cos(\phi_{ee}^s + \phi_{ee}^d) + \cos(\phi_{ee}^s - \phi_{ee}^d)] \\
&+ 2|\varepsilon_{e\mu}^s| |\varepsilon_{\mu e}^d| \cos(\phi_{\mu e}^s + \phi_{\mu e}^d) \\
&+ 2|\varepsilon_{e\tau}^s| |\varepsilon_{\tau e}^d| \cos(\phi_{\tau e}^s + \phi_{\tau e}^d) \\
&+ \mathcal{O}\left(\frac{\Delta m_{31}^2 L}{4E}\right) + \mathcal{O}(\varepsilon^3),
\end{aligned} \tag{29}$$

where we have taken into account also second order terms in  $\varepsilon$ , which may be important in the near detector due

to the large event rates. Eq. (29) corresponds to an overall rescaling of the neutrino flux, which, however, will be hard to detect in a realistic experiment due to the systematical flux uncertainty.

### 3.2. The $\nu_\mu \rightarrow \nu_e$ channel

In the derivation of  $P_{\nu_\mu^s \rightarrow \nu_e^d}$ , we will relax our approximations from the previous section, and take into account also terms of  $\mathcal{O}(s_{13} \Delta m_{21}^2/\Delta m_{31}^2)$ ,  $\mathcal{O}([\Delta m_{21}^2/\Delta m_{31}^2]^2)$ , and  $\mathcal{O}(\varepsilon \Delta m_{21}^2/\Delta m_{31}^2)$ , to reproduce the correct  $\delta_{\text{CP}}$  dependence. For experiments with a relatively short baseline, such as T2K, it is justified to assume vacuum oscillations, if the  $\varepsilon^m$  parameters are  $\lesssim \mathcal{O}(0.1)$  (in Sec. 5, we will discuss cases where this is not true, and we will see that non-standard matter effects can then be large in T2K). The vacuum oscillation probability reads

$$\begin{aligned}
P_{\nu_\mu^s \rightarrow \nu_e^d}^{\text{vac}} &= 4s_{13}^2 s_{23}^2 \sin^2 \frac{\Delta m_{31}^2 L}{4E} \\
&+ \left(\frac{\Delta m_{21}^2}{\Delta m_{31}^2}\right)^2 c_{23}^2 s_{2\times 12}^2 \left(\frac{\Delta m_{31}^2 L}{4E}\right)^2 \\
&+ \frac{\Delta m_{21}^2}{\Delta m_{31}^2} s_{13} s_{2\times 12} s_{2\times 23} \cos \delta_{\text{CP}} \frac{\Delta m_{31}^2 L}{4E} \sin \frac{\Delta m_{31}^2 L}{2E} \\
&- 2\frac{\Delta m_{21}^2}{\Delta m_{31}^2} s_{13} s_{2\times 12} s_{2\times 23} \sin \delta_{\text{CP}} \frac{\Delta m_{31}^2 L}{4E} \sin^2 \frac{\Delta m_{31}^2 L}{4E} \\
&- 4|\varepsilon_{\mu e}^s| s_{13} s_{23} \cos(\phi_{\mu e}^s + \delta_{\text{CP}}) \sin^2 \frac{\Delta m_{31}^2 L}{4E} \\
&- 2|\varepsilon_{\mu e}^s| s_{13} s_{23} \sin(\phi_{\mu e}^s + \delta_{\text{CP}}) \sin \frac{\Delta m_{31}^2 L}{2E} \\
&- 4|\varepsilon_{\mu e}^d| s_{13} c_{2\times 23} s_{23} \cos(\phi_{\mu e}^d + \delta_{\text{CP}}) \sin^2 \frac{\Delta m_{31}^2 L}{4E} \\
&- 2|\varepsilon_{\mu e}^d| s_{13} s_{23} \sin(\phi_{\mu e}^d + \delta_{\text{CP}}) \sin \frac{\Delta m_{31}^2 L}{2E} \\
&+ 4|\varepsilon_{\tau e}^d| s_{13} s_{2\times 23} s_{23} \cos(\phi_{\tau e}^d + \delta_{\text{CP}}) \sin^2 \frac{\Delta m_{31}^2 L}{4E} \\
&- |\varepsilon_{\mu e}^s| \frac{\Delta m_{21}^2}{\Delta m_{31}^2} s_{2\times 12} c_{23} \sin \phi_{\mu e}^s \frac{\Delta m_{31}^2 L}{2E} \\
&+ 2|\varepsilon_{\mu e}^d| \frac{\Delta m_{21}^2}{\Delta m_{31}^2} s_{2\times 12} s_{23}^2 c_{23} \cos \phi_{\mu e}^d \frac{\Delta m_{31}^2 L}{4E} \sin \frac{\Delta m_{31}^2 L}{2E} \\
&- |\varepsilon_{\mu e}^d| \frac{\Delta m_{21}^2}{\Delta m_{31}^2} s_{2\times 12} c_{23} \sin \phi_{\mu e}^d \frac{\Delta m_{31}^2 L}{2E} \\
&\cdot \left[1 - 2s_{23}^2 \sin^2 \frac{\Delta m_{31}^2 L}{2E}\right] \\
&+ 2|\varepsilon_{\tau e}^d| \frac{\Delta m_{21}^2}{\Delta m_{31}^2} s_{2\times 12} s_{23} c_{23}^2 \cos \phi_{\mu e}^d \frac{\Delta m_{31}^2 L}{4E} \sin \frac{\Delta m_{31}^2 L}{2E} \\
&+ 2|\varepsilon_{\tau e}^d| \frac{\Delta m_{21}^2}{\Delta m_{31}^2} s_{2\times 12} s_{23} c_{23}^2 \sin \phi_{\mu e}^d \frac{\Delta m_{31}^2 L}{2E} \sin^2 \frac{\Delta m_{31}^2 L}{4E} \\
&+ \mathcal{O}\left(\left[\frac{\Delta m_{21}^2}{\Delta m_{31}^2}\right]^3\right) + \mathcal{O}\left(\left[\frac{\Delta m_{21}^2}{\Delta m_{31}^2}\right]^2 s_{13}\right) + \mathcal{O}\left(\frac{\Delta m_{21}^2}{\Delta m_{31}^2} s_{13}^2\right)
\end{aligned}$$

$$\begin{aligned}
& + \mathcal{O}(s_{13}^3) + \mathcal{O}\left(\varepsilon\left[\frac{\Delta m_{21}^2}{\Delta m_{31}^2}\right]^2\right) + \mathcal{O}\left(\varepsilon\tilde{s}_{13}\frac{\Delta m_{21}^2}{\Delta m_{31}^2}\right) \\
& + \mathcal{O}(\varepsilon s_{13}^2) + \mathcal{O}(\varepsilon^2). \tag{30}
\end{aligned}$$

The corresponding expression for the near detector is

$$\begin{aligned}
P_{\nu_\mu^s \rightarrow \nu_e^d}^{\text{vac,ND}} &= |\varepsilon_{\mu e}^s|^2 + |\varepsilon_{\mu e}^d|^2 + 2|\varepsilon_{\mu e}^s||\varepsilon_{\mu e}^d| \cos(\phi_{\mu e}^s - \phi_{\mu e}^d) \\
& + \mathcal{O}\left(\frac{\Delta m_{31}^2 L}{4E}\right) + \mathcal{O}(\varepsilon^3). \tag{31}
\end{aligned}$$

If the baseline is longer, as is the case e.g. in  $\text{NO}\nu\text{A}$ , matter effects are important. To keep the notation concise in this case, we define the effective 13-mixing angle in matter, which is given to lowest order by

$$\tilde{s}_{13} \equiv \frac{\Delta m_{31}^2}{\Delta m_{31}^2 - a_{\text{CC}}} s_{13} + \mathcal{O}(s_{13}^2). \tag{32}$$

The oscillation probability is then

$$\begin{aligned}
P_{\nu_\mu^s \rightarrow \nu_e^d}^{\text{mat}} &= 4\tilde{s}_{13}^2 s_{23}^2 \sin^2 \frac{(\Delta m_{31}^2 - a_{\text{CC}})L}{4E} \\
& + \left(\frac{\Delta m_{21}^2}{\Delta m_{31}^2}\right)^2 c_{23}^2 s_{2\times 12}^2 \left(\frac{\Delta m_{31}^2}{a_{\text{CC}}}\right)^2 \sin^2 \frac{a_{\text{CC}}L}{4E} \\
& - \frac{\Delta m_{21}^2}{\Delta m_{31}^2} \tilde{s}_{13} s_{2\times 12} s_{2\times 23} \cos \delta_{\text{CP}} \frac{\Delta m_{31}^2}{a_{\text{CC}}} \left[ \sin^2 \frac{a_{\text{CC}}L}{4E} - \sin^2 \frac{\Delta m_{31}^2 L}{4E} + \sin^2 \frac{(\Delta m_{31}^2 - a_{\text{CC}})L}{4E} \right] \\
& - \frac{1}{2} \frac{\Delta m_{21}^2}{\Delta m_{31}^2} \tilde{s}_{13} s_{2\times 12} s_{2\times 23} \sin \delta_{\text{CP}} \frac{\Delta m_{31}^2}{a_{\text{CC}}} \left[ \sin \frac{a_{\text{CC}}L}{2E} - \sin \frac{\Delta m_{31}^2 L}{2E} + \sin \frac{(\Delta m_{31}^2 - a_{\text{CC}})L}{2E} \right] \\
& - 4|\varepsilon_{\mu e}^s| \tilde{s}_{13} s_{23} \cos(\phi_{\mu e}^s + \delta_{\text{CP}}) \sin^2 \frac{(\Delta m_{31}^2 - a_{\text{CC}})L}{4E} \\
& - 2|\varepsilon_{\mu e}^s| \tilde{s}_{13} s_{23} \sin(\phi_{\mu e}^s + \delta_{\text{CP}}) \sin \frac{(\Delta m_{31}^2 - a_{\text{CC}})L}{2E} \\
& + 4|\varepsilon_{\mu e}^d| \tilde{s}_{13} s_{23} \cos(\phi_{\mu e}^d + \delta_{\text{CP}}) \left[ c_{23}^2 \sin^2 \frac{a_{\text{CC}}L}{4E} - c_{23}^2 \sin^2 \frac{\Delta m_{31}^2 L}{4E} + s_{23}^2 \sin^2 \frac{(\Delta m_{31}^2 - a_{\text{CC}})L}{4E} \right] \\
& + 2|\varepsilon_{\mu e}^d| \tilde{s}_{13} s_{23} \sin(\phi_{\mu e}^d + \delta_{\text{CP}}) \left[ c_{23}^2 \sin \frac{a_{\text{CC}}L}{2E} - c_{23}^2 \sin \frac{\Delta m_{31}^2 L}{2E} - s_{23}^2 \sin \frac{(\Delta m_{31}^2 - a_{\text{CC}})L}{2E} \right] \\
& - 4|\varepsilon_{\tau e}^d| \tilde{s}_{13} s_{23}^2 c_{23} \cos(\phi_{\tau e}^d + \delta_{\text{CP}}) \left[ \sin^2 \frac{a_{\text{CC}}L}{4E} - \sin^2 \frac{\Delta m_{31}^2 L}{4E} - \sin^2 \frac{(\Delta m_{31}^2 - a_{\text{CC}})L}{4E} \right] \\
& - 2|\varepsilon_{\tau e}^d| \tilde{s}_{13} s_{23}^2 c_{23} \sin(\phi_{\tau e}^d + \delta_{\text{CP}}) \left[ \sin \frac{a_{\text{CC}}L}{2E} - \sin \frac{\Delta m_{31}^2 L}{2E} + \sin \frac{(\Delta m_{31}^2 - a_{\text{CC}})L}{2E} \right] \\
& - 4|\varepsilon_{e\mu}^m| \tilde{s}_{13} s_{23} c_{23}^2 \cos(\phi_{e\mu}^m + \delta_{\text{CP}}) \left[ \sin^2 \frac{a_{\text{CC}}L}{4E} - \sin^2 \frac{\Delta m_{31}^2 L}{4E} + \sin^2 \frac{(\Delta m_{31}^2 - a_{\text{CC}})L}{4E} \right] \\
& - 2|\varepsilon_{e\mu}^m| \tilde{s}_{13} s_{23} c_{23}^2 \sin(\phi_{e\mu}^m + \delta_{\text{CP}}) \left[ \sin \frac{a_{\text{CC}}L}{2E} - \sin \frac{\Delta m_{31}^2 L}{2E} + \sin \frac{(\Delta m_{31}^2 - a_{\text{CC}})L}{2E} \right] \\
& + 8|\varepsilon_{e\mu}^m| \tilde{s}_{13} s_{23}^3 \cos(\phi_{e\mu}^m + \delta_{\text{CP}}) \frac{a_{\text{CC}}}{\Delta m_{31}^2 - a_{\text{CC}}} \sin^2 \frac{(\Delta m_{31}^2 - a_{\text{CC}})L}{4E} \\
& + 4|\varepsilon_{e\tau}^m| \tilde{s}_{13} s_{23}^2 c_{23} \cos(\phi_{e\tau}^m + \delta_{\text{CP}}) \left[ \sin^2 \frac{a_{\text{CC}}L}{4E} - \sin^2 \frac{\Delta m_{31}^2 L}{4E} + \sin^2 \frac{(\Delta m_{31}^2 - a_{\text{CC}})L}{4E} \right] \\
& + 2|\varepsilon_{e\tau}^m| \tilde{s}_{13} s_{23}^2 c_{23} \sin(\phi_{e\tau}^m + \delta_{\text{CP}}) \left[ \sin \frac{a_{\text{CC}}L}{2E} - \sin \frac{\Delta m_{31}^2 L}{2E} + \sin \frac{(\Delta m_{31}^2 - a_{\text{CC}})L}{2E} \right] \\
& + 8|\varepsilon_{e\tau}^m| \tilde{s}_{13} s_{23}^2 c_{23} \cos(\phi_{e\tau}^m + \delta_{\text{CP}}) \frac{a_{\text{CC}}}{\Delta m_{31}^2 - a_{\text{CC}}} \sin^2 \frac{(\Delta m_{31}^2 - a_{\text{CC}})L}{4E} \\
& + 2|\varepsilon_{\mu e}^s| \frac{\Delta m_{21}^2}{\Delta m_{31}^2} s_{2\times 12} c_{23} \cos \phi_{\mu e}^s \frac{\Delta m_{31}^2}{a_{\text{CC}}} \sin^2 \frac{a_{\text{CC}}L}{4E} \\
& - |\varepsilon_{\mu e}^s| \frac{\Delta m_{21}^2}{\Delta m_{31}^2} s_{2\times 12} c_{23} \sin \phi_{\mu e}^s \frac{\Delta m_{31}^2}{a_{\text{CC}}} \sin \frac{a_{\text{CC}}L}{2E}
\end{aligned}$$



$$\begin{aligned}
& - 2|\epsilon_{\mu e}^d| \frac{\Delta m_{21}^2}{\Delta m_{31}^2} s_{2 \times 12} c_{23} \cos \phi_{\mu e}^d \frac{\Delta m_{31}^2}{a_{CC}} \left[ c_{23}^2 \sin^2 \frac{a_{CC} L}{4E} - s_{23}^2 \sin^2 \frac{\Delta m_{31}^2 L}{4E} + s_{23}^2 \sin^2 \frac{(\Delta m_{31}^2 - a_{CC}) L}{4E} \right] \\
& - |\epsilon_{\mu e}^d| \frac{\Delta m_{21}^2}{\Delta m_{31}^2} s_{2 \times 12} c_{23} \sin \phi_{\mu e}^d \frac{\Delta m_{31}^2}{a_{CC}} \left[ c_{23}^2 \sin \frac{a_{CC} L}{2E} + s_{23}^2 \sin \frac{\Delta m_{31}^2 L}{2E} - s_{23}^2 \sin \frac{(\Delta m_{31}^2 - a_{CC}) L}{2E} \right] \\
& + 2|\epsilon_{\tau e}^d| \frac{\Delta m_{21}^2}{\Delta m_{31}^2} s_{2 \times 12} s_{23} c_{23}^2 \cos \phi_{\tau e}^d \frac{\Delta m_{31}^2}{a_{CC}} \left[ \sin^2 \frac{a_{CC} L}{4E} + \sin^2 \frac{\Delta m_{31}^2 L}{4E} - \sin^2 \frac{(\Delta m_{31}^2 - a_{CC}) L}{4E} \right] \\
& + |\epsilon_{\tau e}^d| \frac{\Delta m_{21}^2}{\Delta m_{31}^2} s_{2 \times 12} s_{23} c_{23}^2 \sin \phi_{\tau e}^d \frac{\Delta m_{31}^2}{a_{CC}} \left[ \sin \frac{a_{CC} L}{2E} - \sin \frac{\Delta m_{31}^2 L}{2E} + \sin \frac{(\Delta m_{31}^2 - a_{CC}) L}{2E} \right] \\
& + 4|\epsilon_{e\mu}^m| \frac{\Delta m_{21}^2}{\Delta m_{31}^2} s_{2 \times 12} c_{23}^3 \cos \phi_{e\mu}^m \frac{\Delta m_{31}^2}{a_{CC}} \sin^2 \frac{a_{CC} L}{4E} \\
& - 2|\epsilon_{e\mu}^m| \frac{\Delta m_{21}^2}{\Delta m_{31}^2} s_{2 \times 12} s_{23}^2 c_{23} \cos \phi_{e\mu}^m \frac{\Delta m_{31}^2}{\Delta m_{31}^2 - a_{CC}} \left[ \sin^2 \frac{a_{CC} L}{4E} - \sin^2 \frac{\Delta m_{31}^2 L}{4E} + \sin^2 \frac{(\Delta m_{31}^2 - a_{CC}) L}{4E} \right] \\
& + |\epsilon_{e\mu}^m| \frac{\Delta m_{21}^2}{\Delta m_{31}^2} s_{2 \times 12} s_{23}^2 c_{23} \sin \phi_{e\mu}^m \frac{\Delta m_{31}^2}{\Delta m_{31}^2 - a_{CC}} \left[ \sin \frac{a_{CC} L}{2E} - \sin \frac{\Delta m_{31}^2 L}{2E} + \sin \frac{(\Delta m_{31}^2 - a_{CC}) L}{2E} \right] \\
& - 4|\epsilon_{e\tau}^m| \frac{\Delta m_{21}^2}{\Delta m_{31}^2} s_{2 \times 12} s_{23} c_{23}^2 \cos \phi_{e\tau}^m \frac{\Delta m_{31}^2}{a_{CC}} \sin^2 \frac{a_{CC} L}{4E} \\
& - 2|\epsilon_{e\tau}^m| \frac{\Delta m_{21}^2}{\Delta m_{31}^2} s_{2 \times 12} s_{23} c_{23}^2 \cos \phi_{e\tau}^m \frac{\Delta m_{31}^2}{\Delta m_{31}^2 - a_{CC}} \left[ \sin^2 \frac{a_{CC} L}{4E} - \sin^2 \frac{\Delta m_{31}^2 L}{4E} + \sin^2 \frac{(\Delta m_{31}^2 - a_{CC}) L}{4E} \right] \\
& + |\epsilon_{e\tau}^m| \frac{\Delta m_{21}^2}{\Delta m_{31}^2} s_{2 \times 12} s_{23} c_{23}^2 \sin \phi_{e\tau}^m \frac{\Delta m_{31}^2}{\Delta m_{31}^2 - a_{CC}} \left[ \sin \frac{a_{CC} L}{2E} - \sin \frac{\Delta m_{31}^2 L}{2E} + \sin \frac{(\Delta m_{31}^2 - a_{CC}) L}{2E} \right] \\
& + \mathcal{O}\left(\left[\frac{\Delta m_{21}^2}{\Delta m_{31}^2}\right]^3\right) + \mathcal{O}\left(\left[\frac{\Delta m_{21}^2}{\Delta m_{31}^2}\right]^2 s_{13}\right) + \mathcal{O}\left(\frac{\Delta m_{21}^2}{\Delta m_{31}^2} s_{13}^2\right) + \mathcal{O}(s_{13}^3) \\
& + \mathcal{O}\left(\varepsilon \left[\frac{\Delta m_{21}^2}{\Delta m_{31}^2}\right]^2\right) + \mathcal{O}\left(\varepsilon s_{13} \frac{\Delta m_{21}^2}{\Delta m_{31}^2}\right) + \mathcal{O}(\varepsilon s_{13}^2) + \mathcal{O}(\varepsilon^2). \tag{33}
\end{aligned}$$

Most of the  $\mathcal{O}(\Delta m_{21}^2/\Delta m_{31}^2)$  terms contain factors of  $\Delta m_{31}^2/a_{CC}$ , which can be large at low matter densities, and might therefore seem to spoil the accuracy of the expansion in this case. However, the oscillatory terms in square brackets become small as  $\Delta m_{31}^2/a_{CC}$  becomes large, so that overall, the  $\mathcal{O}(\Delta m_{21}^2/\Delta m_{31}^2)$  terms remain subdominant even if the vacuum limit is approached.

### 3.3. The $\nu_\mu \rightarrow \nu_\mu$ channel

For  $P_{\nu_\mu^s \rightarrow \nu_\mu^d}$ , we obtain

$$\begin{aligned}
P_{\nu_\mu^s \rightarrow \nu_\mu^d}^{\text{vac}} &= 1 - s_{2 \times 23}^2 \sin^2 \frac{\Delta m_{31}^2 L}{4E} \\
&+ 2|\epsilon_{\mu\mu}^s| \cos \phi_{\mu\mu}^s + 2|\epsilon_{\mu\mu}^d| \cos \phi_{\mu\mu}^d \\
&- \left[ 2|\epsilon_{\mu\mu}^s| \cos \phi_{\mu\mu}^s + 2|\epsilon_{\mu\mu}^d| \cos \phi_{\mu\mu}^d \right] s_{2 \times 23}^2 \sin^2 \frac{\Delta m_{31}^2 L}{4E} \\
&- 2 \left( |\epsilon_{\mu\tau}^s| \cos \phi_{\mu\tau}^s + |\epsilon_{\tau\mu}^d| \cos \phi_{\tau\mu}^d \right) c_{2 \times 23} s_{2 \times 23} \sin^2 \frac{\Delta m_{31}^2 L}{4E} \\
&+ \left( |\epsilon_{\mu\tau}^s| \sin \phi_{\mu\tau}^s + |\epsilon_{\tau\mu}^d| \sin \phi_{\tau\mu}^d \right) s_{2 \times 23} \sin \frac{\Delta m_{31}^2 L}{2E} \\
&+ \mathcal{O}\left(\frac{\Delta m_{21}^2}{\Delta m_{31}^2}\right) + \mathcal{O}(s_{13}) + \mathcal{O}(\varepsilon^2). \tag{34}
\end{aligned}$$

in vacuum, and

$$\begin{aligned}
P_{\nu_\mu^s \rightarrow \nu_\mu^d}^{\text{mat}} &= 1 - s_{2 \times 23}^2 \sin^2 \frac{\Delta m_{31}^2 L}{4E} \\
&+ 2|\epsilon_{\mu\mu}^s| \cos \phi_{\mu\mu}^s + 2|\epsilon_{\mu\mu}^d| \cos \phi_{\mu\mu}^d
\end{aligned}$$

$$\begin{aligned}
& - \left[ 2|\epsilon_{\mu\mu}^s| \cos \phi_{\mu\mu}^s + 2|\epsilon_{\mu\mu}^d| \cos \phi_{\mu\mu}^d \right] s_{2\times 23}^2 \sin^2 \frac{\Delta m_{31}^2 L}{4E} \\
& - 2 \left( |\epsilon_{\mu\tau}^s| \cos \phi_{\mu\tau}^s + |\epsilon_{\tau\mu}^d| \cos \phi_{\tau\mu}^d \right) c_{2\times 23} s_{2\times 23} \sin^2 \frac{\Delta m_{31}^2 L}{4E} \\
& + \left( |\epsilon_{\mu\tau}^s| \sin \phi_{\mu\tau}^s + |\epsilon_{\tau\mu}^d| \sin \phi_{\tau\mu}^d \right) s_{2\times 23} \sin \frac{\Delta m_{31}^2 L}{2E} \\
& - |\epsilon_{\mu\tau}^m| \left[ s_{2\times 23}^3 \cos \phi_{\mu\tau}^m \frac{a_{CC} L}{2E} \sin \frac{\Delta m_{31}^2 L}{2E} + 4s_{2\times 23} c_{2\times 23}^2 \cos \phi_{\mu\tau}^m \frac{a_{CC}}{\Delta m_{31}^2} \sin^2 \frac{\Delta m_{31}^2 L}{4E} \right] \\
& + \frac{1}{2} |\epsilon_{\mu\mu}^m| \left[ s_{2\times 23}^2 c_{2\times 23} \frac{a_{CC} L}{2E} \sin \frac{\Delta m_{31}^2 L}{2E} - 4s_{2\times 23}^2 c_{2\times 23} \frac{a_{CC}}{\Delta m_{31}^2} \sin^2 \frac{\Delta m_{31}^2 L}{4E} \right] \\
& - \frac{1}{2} |\epsilon_{\tau\tau}^m| \left[ s_{2\times 23}^2 c_{2\times 23} \frac{a_{CC} L}{2E} \sin \frac{\Delta m_{31}^2 L}{2E} - 4s_{2\times 23}^2 c_{2\times 23} \frac{a_{CC}}{\Delta m_{31}^2} \sin^2 \frac{\Delta m_{31}^2 L}{4E} \right] \\
& + \mathcal{O}\left(\frac{\Delta m_{21}^2}{\Delta m_{31}^2}\right) + \mathcal{O}(s_{13}) + \mathcal{O}(\varepsilon^2). \tag{35}
\end{aligned}$$

in matter.

### 3.4. Interpretation

To understand the physical origin of the formulas derived in the previous sections, let us consider Figs. 1 – 3, where we show schematically the possible reaction chains that a neutrino can follow before its detection. We also indicate the respective suppression factors of the transition amplitude, but to simplify the discussion and to improve the clarity of the figures, we do not explicitly show contributions proportional to  $\Delta m_{21}^2/\Delta m_{31}^2$ , which would appear in concurrence to the  $\theta_{13}$ -suppressed processes if  $\theta_{13}$  is very small. Dotted lines indicate suppression due to standard effects, while dashed lines represent transitions that are suppressed by the non-standard parameters. The thick blue (black) paths are those followed by the standard oscillation channels, while light gray lines indicate paths that are suppressed by more than one  $\varepsilon$  parameter, and are therefore mostly negligible. In Tab. II we summarize the same considerations in tabular form. In the first part of the discussion, we will assume  $\varepsilon^s$  and  $\varepsilon^d$  to be completely independent in order to keep the discussion as general as possible. The constraints from Eqs. (16) and (17) will only be implemented afterwards.

On the reactor side, we can read off from Fig. 1 and Tab. II, that, in the presence of just one type of non-standard interaction, only  $\varepsilon_{ee}^s$ ,  $\varepsilon_{e\mu}^s$ ,  $\varepsilon_{e\tau}^s$ ,  $\varepsilon_{ee}^d$ ,  $\varepsilon_{\mu e}^d$ , and  $\varepsilon_{\tau e}^d$  are relevant. Of these,  $\varepsilon_{ee}^s$  and  $\varepsilon_{ee}^d$  have an  $\mathcal{O}(\varepsilon)$  effect which could even exceed standard oscillations if it were not for the near detector, where these parameters would induce a similar effect as in the far detector. Since the absolute reactor neutrino flux is not known precisely, the measurement relies on the *relative* counting rates in both detectors, so that the impact of  $\varepsilon_{ee}^s$  and  $\varepsilon_{ee}^d$  is canceled. The remaining NSI,  $\varepsilon_{e\mu}^s$ ,  $\varepsilon_{e\tau}^s$ ,  $\varepsilon_{\mu e}^d$ , and  $\varepsilon_{\tau e}^d$ , contribute to the oscillation probability at  $\mathcal{O}(\varepsilon \sin 2\theta_{13})$  (or at  $\mathcal{O}(\varepsilon \sin 2\theta_{13} + \varepsilon^2)$ , if the constraint  $\varepsilon_{e\alpha}^s = \varepsilon_{\alpha e}^{d*}$  from Eq. (16) is implemented). This can be comparable to the standard term, so that these NSI are expected to have

a large impact on the far detector. They do not affect the near detector as long as only one of them is present, but if Eq. (16) is taken into account, the near detector will receive an  $\mathcal{O}(\varepsilon^2)$  contribution that can be important in some situations. All these considerations are nicely confirmed by Eq. (28).

For a superbeam experiment, Fig. 2 and Tab. II show that, as long as only one type of NSI is taken into account,  $\varepsilon_{\mu e}^s$ ,  $\varepsilon_{\mu\mu}^s$ ,  $\varepsilon_{\mu\tau}^s$  can affect the production process, while  $\varepsilon_{ee}^d$ ,  $\varepsilon_{e\mu}^d$ ,  $\varepsilon_{\mu e}^d$ ,  $\varepsilon_{\mu\mu}^d$ ,  $\varepsilon_{\tau e}^d$ , and  $\varepsilon_{\tau\mu}^d$  may be important in the detector. The propagation can be affected by all entries of  $\varepsilon^m$ . As for the reactor case, the suppression factors associated with these different processes can be understood from simple physical arguments, which are confirmed in a more rigorous way by Eqs. (30) and (34). Let us discuss the different types of NSI in more detail:

- $\varepsilon_{e\mu}^d$  and  $\varepsilon_{\tau\mu}^d$  affect only the disappearance channel and are therefore irrelevant for the measurement of  $\theta_{13}$  (they may, however, lead to wrong results for the leading atmospheric parameters).
- $\varepsilon_{\mu\mu}^d$  also affects the disappearance channel, but it can also lead to a modified  $\nu_\mu$  rate in the near detector, and therefore to wrong assumptions on the initial neutrino flux. This, in turn, could lead to a misinterpretation of the far detector appearance measurement, so that the  $\theta_{13}$  measurement is influenced indirectly. The effect in the near detector is suppressed by  $\varepsilon$ , so it will affect the far detector analysis only at the subleading level of  $\varepsilon \sin^2 2\theta_{13}$ .
- $\varepsilon_{\mu\mu}^s$ ,  $\varepsilon_{\mu\tau}^s$  and  $\varepsilon_{ee}^d$  are relevant for the appearance channel, but the corresponding *amplitude* is suppressed by  $\varepsilon \sin 2\theta_{13}$ , so that in the oscillation *probability*, we would obtain a subdominant contribution of  $\mathcal{O}(\varepsilon \sin^2 2\theta_{13})$  from the interference of the standard and non-standard terms.
- $\varepsilon_{\mu e}^s$ ,  $\varepsilon_{\mu e}^d$ , and  $\varepsilon_{\tau e}^d$  have *amplitudes* of  $\mathcal{O}(\varepsilon)$ , i.e.

NSI	Reactor		Superbeam		
	$\bar{\nu}_e$ disappearance	Effect in ND	$\nu_e$ appearance	$\nu_\mu$ disappearance	Effect in ND
None	1	—	$\sin 2\theta_{13}$	$\cos(\Delta m_{31}^2 L/4E)$	—
$\varepsilon_{ee}^s$	$\varepsilon$	modified $\bar{\nu}_e$ flux	—	—	—
$\varepsilon_{e\mu}^s$	$\varepsilon \sin 2\theta_{13}$	—	—	—	—
$\varepsilon_{e\tau}^s$	$\varepsilon \sin 2\theta_{13}$	—	—	—	—
$\varepsilon_{\mu e}^s$	—	—	$\varepsilon$	$\varepsilon \sin 2\theta_{13}$	modified $\nu_e$ flux
$\varepsilon_{\mu\mu}^s$	—	—	$\varepsilon \sin 2\theta_{13}$	$\varepsilon \cos(\Delta m_{31}^2 L/4E)$	modified $\nu_\mu$ flux
$\varepsilon_{\mu\tau}^s$	—	—	$\varepsilon \sin 2\theta_{13}$	$\varepsilon$	—
$\varepsilon_{\tau e}^s$	—	—	—	—	—
$\varepsilon_{\tau\mu}^s$	—	—	—	—	—
$\varepsilon_{\tau\tau}^s$	—	—	—	—	—
$\varepsilon_{ee}^d$	$\varepsilon$	modified $\bar{\nu}_e$ flux	$\varepsilon \sin 2\theta_{13}$	—	—
$\varepsilon_{e\mu}^d$	—	—	—	$\varepsilon \sin 2\theta_{13}$	—
$\varepsilon_{e\tau}^d$	—	—	—	—	—
$\varepsilon_{\mu e}^d$	$\varepsilon \sin 2\theta_{13}$	—	$\varepsilon \cos(\Delta m_{31}^2 L/4E)$	—	modified $\nu_e$ flux
$\varepsilon_{\mu\mu}^d$	—	—	—	$\varepsilon \cos(\Delta m_{31}^2 L/4E)$	modified $\nu_\mu$ flux
$\varepsilon_{\mu\tau}^d$	—	—	—	—	—
$\varepsilon_{\tau e}^d$	$\varepsilon \sin 2\theta_{13}$	—	$\varepsilon$	—	—
$\varepsilon_{\tau\mu}^d$	—	—	—	$\varepsilon$	—
$\varepsilon_{\tau\tau}^d$	—	—	—	—	—
$\varepsilon_{ee}^s = \varepsilon_{ee}^{d*}$	$\varepsilon$	modified $\bar{\nu}_e$ flux	$\varepsilon \sin 2\theta_{13}$	—	—
$\varepsilon_{e\mu}^s = \varepsilon_{e\mu}^{d*}$	$\varepsilon \sin 2\theta_{13} + \varepsilon^2$	modified $\bar{\nu}_e$ flux	$\varepsilon \cos(\Delta m_{31}^2 L/4E)$	—	modified $\nu_e$ flux
$\varepsilon_{e\tau}^s = \varepsilon_{e\tau}^{d*}$	$\varepsilon \sin 2\theta_{13} + \varepsilon^2$	modified $\bar{\nu}_e$ flux	$\varepsilon$	—	—
$\varepsilon_{\mu e}^s = \varepsilon_{\mu e}^{d*}$	—	—	$\varepsilon$	$\varepsilon \sin 2\theta_{13} + \varepsilon^2$	modified $\nu_e$ flux
$\varepsilon_{\mu\mu}^s = \varepsilon_{\mu\mu}^{d*}$	—	—	$\varepsilon \sin 2\theta_{13}$	$\varepsilon \cos(\Delta m_{31}^2 L/4E)$	modified $\nu_\mu$ flux
$\varepsilon_{\mu\tau}^s = \varepsilon_{\mu\tau}^{d*}$	—	—	$\varepsilon \sin 2\theta_{13}$	$\varepsilon$	—
$\varepsilon_{ee}^m$	—	—	$\varepsilon \sin 2\theta_{13}$	$\varepsilon \sin^2 2\theta_{13}$	—
$\varepsilon_{e\mu}^m$	—	—	$\varepsilon$	$\varepsilon \sin 2\theta_{13}$	—
$\varepsilon_{e\tau}^m$	—	—	$\varepsilon$	$\varepsilon \sin 2\theta_{13}$	—
$\varepsilon_{\mu\mu}^m$	—	—	$\varepsilon \sin 2\theta_{13}$	$\varepsilon \cos 2\theta_{23}$ <sup>a</sup>	—
$\varepsilon_{\mu\tau}^m$	—	—	$\varepsilon \sin 2\theta_{13}$	$\varepsilon$	—
$\varepsilon_{\tau\tau}^m$	—	—	$\varepsilon \sin 2\theta_{13}$	$\varepsilon \cos 2\theta_{23}$ <sup>a</sup>	—

<sup>a</sup>The factor  $\cos 2\theta_{23}$  cannot be derived from Fig. 3, but only from Eq. (35).

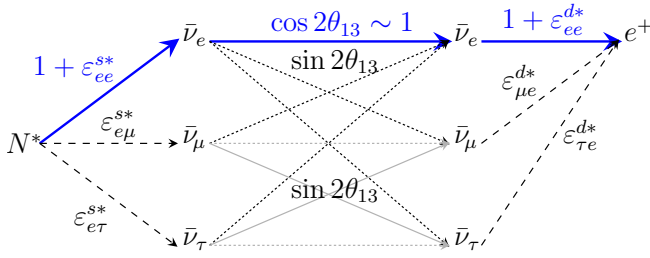
Table II: Classification of the reparameterized non-standard interactions  $\varepsilon^s$ ,  $\varepsilon^d$ , and  $\varepsilon^m$  according to their impact on the transition amplitudes for reactor and superbeam experiments. For each NSI coupling, only the leading order effect is shown. The framed entries highlight those terms that are most relevant to the determination of  $\theta_{13}$  (see text for details).

they contribute to the appearance *probability* on the level of  $\varepsilon \sin 2\theta_{13}$ , which can be comparable to the leading contribution  $\sim \sin^2 2\theta_{13}$ .  $\varepsilon_{\mu e}^d$ , however, is suppressed by a factor of  $\cos(\Delta m_{31}^2 L/4E)$ , which is small at the first atmospheric maximum around which the beam is centered. Note also that the modified  $\nu_e$  flux in the near detector that is expected in the presence of  $\varepsilon_{\mu e}^s$  or  $\varepsilon_{\mu e}^d$  can help to actually detect the NSI, although part of it may be misinterpreted as a systematical error on the intrinsic beam background.

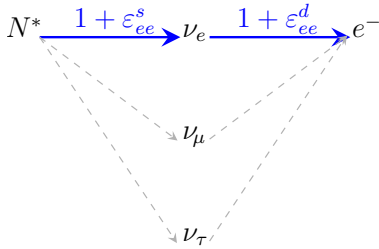
- Of the non-standard matter effects, only  $\varepsilon_{e\mu}^m$  and

$\varepsilon_{e\tau}^m$  contribute at leading order to the appearance probability  $P_{\nu_\mu^s \rightarrow \nu_e^d}^{\text{mat}}$ . Of these,  $\varepsilon_{e\mu}^m$  is already strongly constrained experimentally [47], and so is not expected to have a large impact on reactor and superbeam experiments.  $\varepsilon_{e\tau}^m$ , on the other hand, could contribute significantly to the superbeam appearance channel, in accordance with [8, 30]. All other non-standard matter effects are suppressed by an additional power of  $s_{13}$ , (or, more correctly,  $\tilde{s}_{13}$ , which is, however, still small since we are far from the MSW resonance).

It is interesting to observe that the sensitivity to



(a)



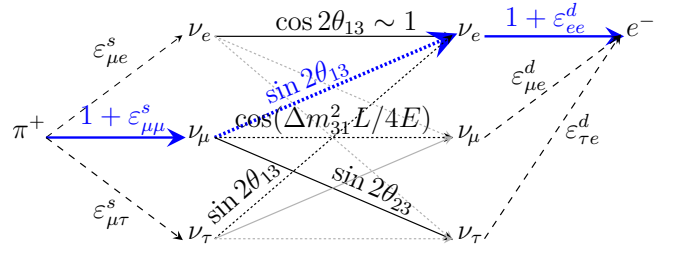
(b)

Figure 1: Possible contributions of  $\varepsilon^s$  and  $\varepsilon^d$  to the event rate in the far detector (a), and the near detector (b) of a reactor  $\bar{\nu}_e$  disappearance experiment. Thick blue lines indicate the reaction chain for standard oscillations. Dotted lines indicate processes that are suppressed by standard three-flavor effects proportional to  $\theta_{13}$  or  $\Delta m_{21}^2/\Delta m_{31}^2$ , while dashed lines represent transitions that are suppressed due to non-standard interactions. Paths which would only be accessible in the presence of two different non-standard effects, are shown in light gray since they are usually subdominant.

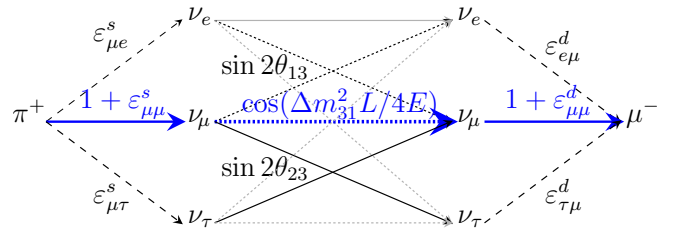
$\varepsilon_{ee}^m$  is very weak, although this type of interaction corresponds to a simple rescaling of the standard MSW potential. However, it is not a leading order effect, and therefore does not appear in our approximate formula, Eq. (33).

- In  $P_{\nu_\mu^s \rightarrow \nu_\mu^d}^{\text{mat}}$ , the dominant matter effect is  $\varepsilon_{\mu\tau}^m$ , and since there is no  $\theta_{13}$  suppression from the interference with the standard amplitude, this effect is even stronger than those in  $P_{\nu_\mu^s \rightarrow \nu_e^d}^{\text{mat}}$ . Note that, from Fig. 3, one might expect  $\varepsilon_{\mu\mu}^m$  and  $\varepsilon_{\tau\tau}^m$  to be of similar strength as  $\varepsilon_{\mu\tau}^m$ , but when one performs the calculation, it turns out that an additional suppression factor  $c_{2 \times 23}$  appears (cf. Eq. (35)).
- The implementation of the constraints  $\varepsilon_{e\alpha}^s = \varepsilon_{\alpha e}^{d*}$  (Eq. (16)) and  $|\varepsilon_{\mu\alpha}^s| \gtrsim |\varepsilon_{\alpha\mu}^d|$  (Eq. (17)) does not lead to any new effects, except for the appearance of an additional  $\varepsilon^2$  term in the disappearance channel for  $\varepsilon_{\mu e}^s = \varepsilon_{e\mu}^{d*}$ .

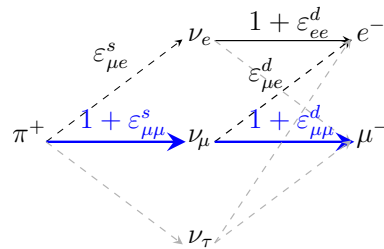
Let us finally emphasize the crucial importance of the standard and non-standard phases in the oscillation probabilities: The formulas from Secs. 3.1 – 3.3 reveal that un-



(a)



(b)



(c)

Figure 2: Possible contributions of  $\varepsilon^s$  and  $\varepsilon^d$  to the event rate in a superbeam experiment for the appearance channel (a), the disappearance channel (b), and in the near detector (c). The meaning of the colors and line styles is the same as in Fig. 1.

favorable phase combinations may suppress non-standard effects, even if the modulus of the corresponding  $\varepsilon$  parameter is large.

#### 4. SIMULATION OF REACTOR AND SUPERBEAM EXPERIMENTS

To fully assess the high-level consequences of non-standard interactions for realistic reactor and superbeam experiments, we have performed numerical simulations using the GLOBES software [69, 70]. We have considered the following scenarios:

- T2K + Double Chooz. Our simulation of the T2K far detector, Super-Kamiokande, is based on [71]. Most parameters are taken from the T2K letter of

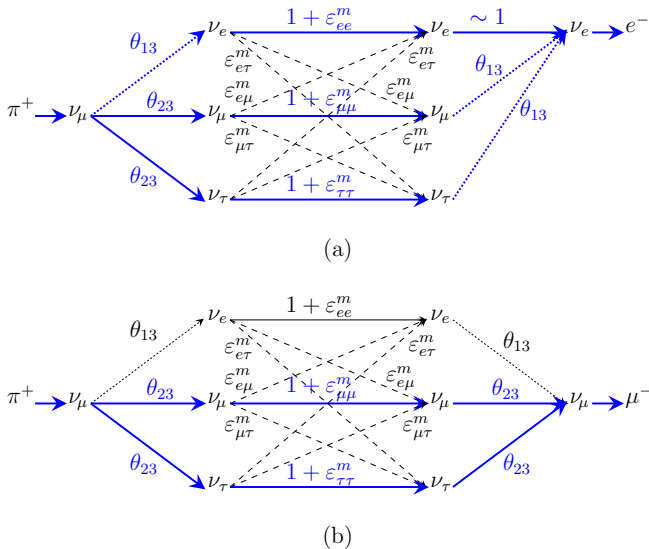


Figure 3: Possible contributions of  $\varepsilon^m$  to the event rate in the superbeam appearance channel (a), and in the corresponding disappearance channel (b). The meaning of the colors and line styles is the same as in Fig. 1.

intent [48], and the systematical uncertainties are based on [72]. We include a separate 1.0 kt water Čerenkov near detector with similar properties as the far detector, and similar systematical uncertainties. To model the interplay of the two detectors, we introduce a common 10% uncertainty on the neutrino flux, and a common 20% error on the number of background events in the  $\nu_e$  appearance channel. In the absence of non-standard interactions, these correlated errors would cancel completely, since the total neutrino flux and the background contribution are effectively calibrated by the near detector, but if  $\varepsilon^{s,d} \neq 0$ , this calibration can be wrong, and there may be an observable effect. The neutrino interaction cross sections are taken from [60, 73]. We assume 3 years of neutrino running and 3 years of anti-neutrino running, each with a beam power of 0.77 MW. The fiducial far detector mass is 22.5 kt, and the baseline is 295 km. We consider  $\nu_e$  appearance events as well as the  $\nu_\mu$  disappearance signal. The background for the disappearance channel is made up of neutral current events, while for the appearance measurement, neutral current events, misidentified muons, and the intrinsic beam backgrounds can contribute.

For the simulation of **Double Chooz**, we use the same parameters as in [53], and the cross sections for inverse beta decay are taken from [74]. As for **T2K**, we simulate the near and far detectors separately, but take into account the appropriate correlations between systematical errors. In particular, we introduce a 2.8% flux normalization error, which is correlated between the near and far de-

tectors, uncorrelated 0.6% fiducial mass errors for both detectors, uncorrelated 0.5% energy calibration uncertainties, and an 0.5% bin-to-bin uncorrelated error.

- **NO $\nu$ A + DC-200**, where DC-200 refers to a reactor experiment similar to **Double Chooz**, but with a 200 t far detector [53]. Such a large reactor experiment has a considerable sensitivity not only to the total event rate, but also to distortions of the energy spectrum.

The simulation of the  $\nu_e$  appearance signal in **NO $\nu$ A** is based on [50], while for the  $\nu_\mu$  disappearance channel, we follow [75]. We assume 3 years of neutrino running and 3 years of anti-neutrino running, with a beam power of 1.12 MW. The far detector mass is 25 kt, and the baseline is 812 km, with an average matter density of 2.8 g/cm<sup>3</sup> along the trajectory, while the near detector has a mass of 0.0204 kt, and is located at 1 km from the target. Again, we introduce, in addition to the uncorrelated systematical errors from [50, 75], a correlated 10% uncertainty on the total neutrino flux, and a correlated 20% error on the  $\nu_e$  background.

The parameters and systematical errors of the DC-200 scenario are identical to those of **Double Chooz**.

Unless indicated otherwise, we calculate the respective event rates using the following “true” values for the oscillation parameters [76]:

$$\begin{aligned}
 \sin^2 2\theta_{12}^{\text{true}} &= 0.84, \\
 \sin^2 2\theta_{23}^{\text{true}} &= 1.0, \\
 \sin^2 2\theta_{13}^{\text{true}} &= 0.05, \\
 \delta_{\text{CP}}^{\text{true}} &= 0.0, \\
 (\Delta m_{21}^2)^{\text{true}} &= 7.9 \times 10^{-5} \text{ eV}^2, \\
 (\Delta m_{31}^2)^{\text{true}} &= 2.6 \times 10^{-3} \text{ eV}^2,
 \end{aligned} \tag{36}$$

and assume a normal mass hierarchy. To analyze the simulated data, we follow the statistical procedure described in the appendix of [71], and define the following  $\chi^2$  function<sup>1</sup>

$$\chi^2 = \min_{\lambda} \sum_j^{\text{channel}} \sum_i^{\text{bin}} \frac{|N_{ij}(\lambda^{\text{true}}, \varepsilon^{\text{true}}) - N_{ij}(\lambda, \varepsilon = 0)|^2}{N_{ij}(\lambda^{\text{true}}, \varepsilon^{\text{true}})} + \text{Priors}, \tag{37}$$

where  $N_{ij}$  denotes the number of events in the  $i$ -th energy bin for oscillation channel  $j$ , the vector  $\lambda =$

<sup>1</sup> In the implementation of superbeam experiments, we assume the events to follow the Poisson distribution. However, for illustrative purposes, it is sufficient to consider the more compact approximative Gaussian expression.

$(\theta_{12}, \theta_{13}, \theta_{23}, \delta_{\text{CP}}, \Delta m_{21}^2, \Delta m_{31}^2, \vec{b})$  contains the standard oscillation parameters and the systematical biases  $\vec{b}$ , and  $\varepsilon$  represents the non-standard parameters. In the fit, we marginalize  $\chi^2$  over all standard oscillation parameters and over the systematical biases, but since we want to study how a standard-oscillation fit gets modified if there are non-standard interactions, we keep the NSI parameters fixed at 0.<sup>2</sup> The prior terms implement external input from other experiments and have the form  $(x - x^{\text{true}})^2/\sigma_x^2$ , where  $x$  stands for any oscillation parameter or systematical bias, and  $\sigma_x$  is the corresponding externally given uncertainty. We assume  $\theta_{12}$  to be known to within 10%, and  $\Delta m_{21}^2$  to within 5% from solar and reactor experiments [76]. When analyzing the reactor experiment alone, we additionally assume a 15% uncertainty on  $\theta_{23}$  and a 5% error on  $\Delta m_{31}^2$ . Beam experiments are themselves sensitive to  $\theta_{23}$  and  $\Delta m_{31}^2$ , so we omit these priors for them.

## 5. NSI-INDUCED OFFSETS AND DISCREPANCIES IN $\theta_{13}$ FITS

Using the simulation techniques discussed in the previous section, we can now determine the errors that are introduced when non-standard interactions are present in reactor and superbeam experiments, but are not properly taken into account in the respective fits. Possible outcomes of such fits are shown in Fig. 4 for our two scenarios. As “true” parameter values, we have taken  $\sin^2 2\theta_{13} = 0.05$  and  $\delta_{\text{CP}} = \pi$ , and the NSI contribution was assumed to be  $\varepsilon_{e\tau}^m = 0.5e^{-i\pi/2}$  in the upper panel, and  $\varepsilon_{e\tau}^s = \varepsilon_{\tau e}^d = 0.05$  (fulfilling Eq. (16)) in the lower panel. These NSI parameters are rather large, but still consistent with current bounds [31, 47]. According to the discussion in Sec. 3, only the superbeam experiment should be affected in the first case, while in the second case, there should be an impact on both experiments. The shaded areas show the 90% confidence regions for the reactor experiment, while the colored contours are for the superbeam. The data has been calculated under the assumption of a normal mass hierarchy, but the fit has been performed for both the normal mass ordering (solid blue/dark gray contours) and for the inverted ordering (dashed pink/light gray contours). The vertical black line and the colored diamonds represent the respective best fit values, while the black star stands for the assumed “true” parameter values. We have assumed two degrees of freedom for the superbeam experiments, and one degree of freedom for the reactor setups, which are insensitive to  $\delta_{\text{CP}}$ .

It is obvious from the plots that the standard oscillation fit to  $\theta_{13}$  and  $\delta_{\text{CP}}$  can be severely wrong if NSI

are present. This observation is similar to the one made in [34] for a neutrino factory. In the case shown in the upper plots of Fig. 4, the reactor experiment gives the correct best fit value, but the superbeam results conflict with this measurement. In the case of  $\text{NO}\nu\text{A}$ , we even obtain a fit value above the Chooz bound and a fake hint to the mass hierarchy, indicated by the fact that, within the resolution of the plot, the 90% contour reduces to a single point. In the second case (lower plots), both experiments agree very well, but they erroneously seem to rule out the “true”  $\theta_{13}$ .

Of course, the NSI scenarios analyzed in Fig. 4 were only two examples, and a more systematic analysis of non-standard interactions in reactor and superbeam experiments is desirable. This is done in Figs. 5 – 7, where we show how the (standard oscillation)  $\theta_{13}$  fits in T2K/Double Chooz respectively in  $\text{NO}\nu\text{A}/\text{DC-200}$  may be distorted in the presence of non-standard interactions. For each diagram, only one of the independent  $\varepsilon$  parameters was assumed to be non-zero, but we have ensured that Eqs. (16) and (17) are fulfilled. In particular, we did not consider the hypothetical case  $\varepsilon_{\mu\alpha}^s = 0$ ,  $\varepsilon_{\alpha\mu}^d \neq 0$ , but only  $\varepsilon_{\mu\alpha}^s \neq 0$ ,  $\varepsilon_{\alpha\mu}^d = 0$  and  $\varepsilon_{\mu\alpha}^s = \varepsilon_{\alpha\mu}^d \neq 0$ . Moreover we omit all entries of  $\varepsilon^m$  except  $\varepsilon_{e\tau}^m$ , because they are either strongly constrained already ( $\varepsilon_{e\mu}^m$ ), or do not have any impact on the  $\theta_{13}$  measurements ( $\varepsilon_{ee}^m$ ,  $\varepsilon_{\mu\mu}^m$ ,  $\varepsilon_{\mu\tau}^m$ , and  $\varepsilon_{\tau\tau}^m$ ). The modulus of each parameter has been varied between 0 and its current upper bound, which is 0.1 for  $\varepsilon_{\alpha\beta}^{s,d}$  from universality in charged lepton decays [31], and 0.7 for  $\varepsilon_{e\tau}^m$  [47].<sup>3</sup> The complex phases were allowed to vary between 0 and  $2\pi$ . For each combination of  $|\varepsilon|$  and  $\arg(\varepsilon)$ , we have then performed a fit assuming standard oscillations, and the resulting best fit values for  $\theta_{13}$  are shown in the plots. Points giving a good fit (better than  $3\sigma$  in both experiments), are drawn as thick colored lines, with the hue indicating the respective value of  $|\varepsilon|$ . Dark red (dark gray) corresponds to  $|\varepsilon| = 0$ , while yellow (medium gray) corresponds to the upper bound of  $|\varepsilon|$ . Points giving a fit quality worse than  $3\sigma$  are shown by thin light gray lines, and the information on  $|\varepsilon|$  is omitted for them. All computations have been performed for two different “true” values,  $\sin^2 2\theta_{13} = 0.01$  and  $\sin^2 2\theta_{13} = 0.05$ , as indicated by the black stars.

By comparing the plots with Tab. II, we find that our expectations for the impact of the different  $\varepsilon$  parameters from the discussion in Sec. 3 are confirmed. A particularly interesting situation arises for  $\varepsilon_{\tau e}^d$ , because this parameter has a sizeable effect in both, the reactor experiment and the superbeam setup. It is especially dangerous because it induces a similar offset in both experiments, i.e. one would find perfectly consistent  $\theta_{13}$  fits,

<sup>2</sup> Of course, when computing confidence intervals for certain parameters, we have to keep these parameters fixed as well.

<sup>3</sup> Note that, according to the naive estimate from Eq. (7), such large values of  $|\varepsilon|$  would correspond to  $M_{\text{NSI}} \sim \mathcal{O}(100 \text{ GeV})$ . In many models, such low new physics scales are already ruled out, but in our model-independent treatment, they are still viable.

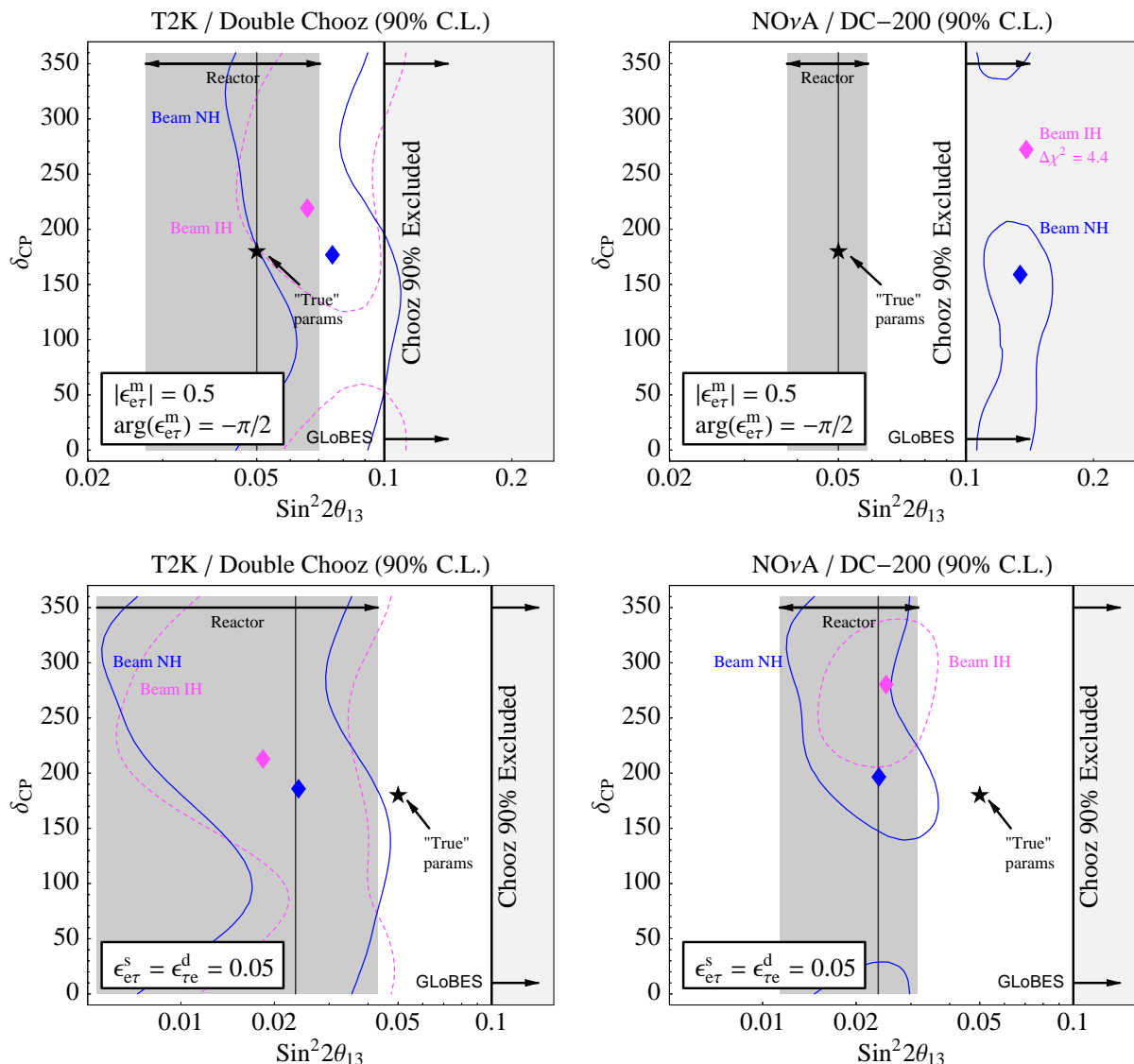


Figure 4: Two examples for the errors that are introduced if non-standard interactions are neglected when fitting  $\theta_{13}$  and  $\delta_{\text{CP}}$  to the data of reactor and superbeam experiment. In the upper plots, a discrepancy arises between the two experiments (the  $\text{NO}\nu\text{A}$  fit is even above the Chooz bound), while in the lower plots, there is a common offset, leading to consistent results, but erroneously “ruling out” the true  $\theta_{13}$  (indicated by the black star) at a high confidence level. The left hand plots are for T2K and Double Chooz, and the right hand ones are for  $\text{NO}\nu\text{A}$  and DC-200. The gray shading represents the 90% confidence region from the reactor experiment, and the vertical black line shows the corresponding best fit value for  $\theta_{13}$ . The 90% contours from the superbeam are shown as solid blue (dark gray) lines for a normal hierarchy fit, and as dashed pink (light gray) lines for an inverted hierarchy fit. The colored diamonds represent the corresponding best fit values. In interpreting the computed  $\chi^2$  values, we have assumed 2 degrees of freedom for the beam experiments, and one degree of freedom for the reactor setups.

which might, however, be far away from the true value.

Other parameters may lead to fit points far from the diagonal, corresponding to seemingly conflicting fits. An interesting case is the  $\varepsilon_{\mu e}^d$  term, for which the non-standard interaction mimics a significantly modified  $\nu_e$  flux in the near detector. This, in turn, leads to a miscalibration of the beam-intrinsic backgrounds, so that, at the far site, many of the actually oscillation-induced  $\nu_e$  events will be mistaken as background. Thus, the fit value for  $\theta_{13}$  becomes too small. However, we can also read off from the plot, that, in this situation, the quality

of the standard oscillation fit becomes so bad that the NSI effect can actually be detected. Note that the curves for large  $|\varepsilon_{\mu e}^d|$  look slightly untidy, because for some parameter values, the smallest  $\chi^2$  is provided by the normal hierarchy fit, while for others the inverted hierarchy fit is marginally better. Therefore, frequent “jumps” between these two solutions occur.

When interpreting Figs. 5 and 6, it is important to keep in mind that the error bars of the experiments considered here are rather large (cf. Fig. 4), so that even sizeable deviations from the diagonals will in most cases

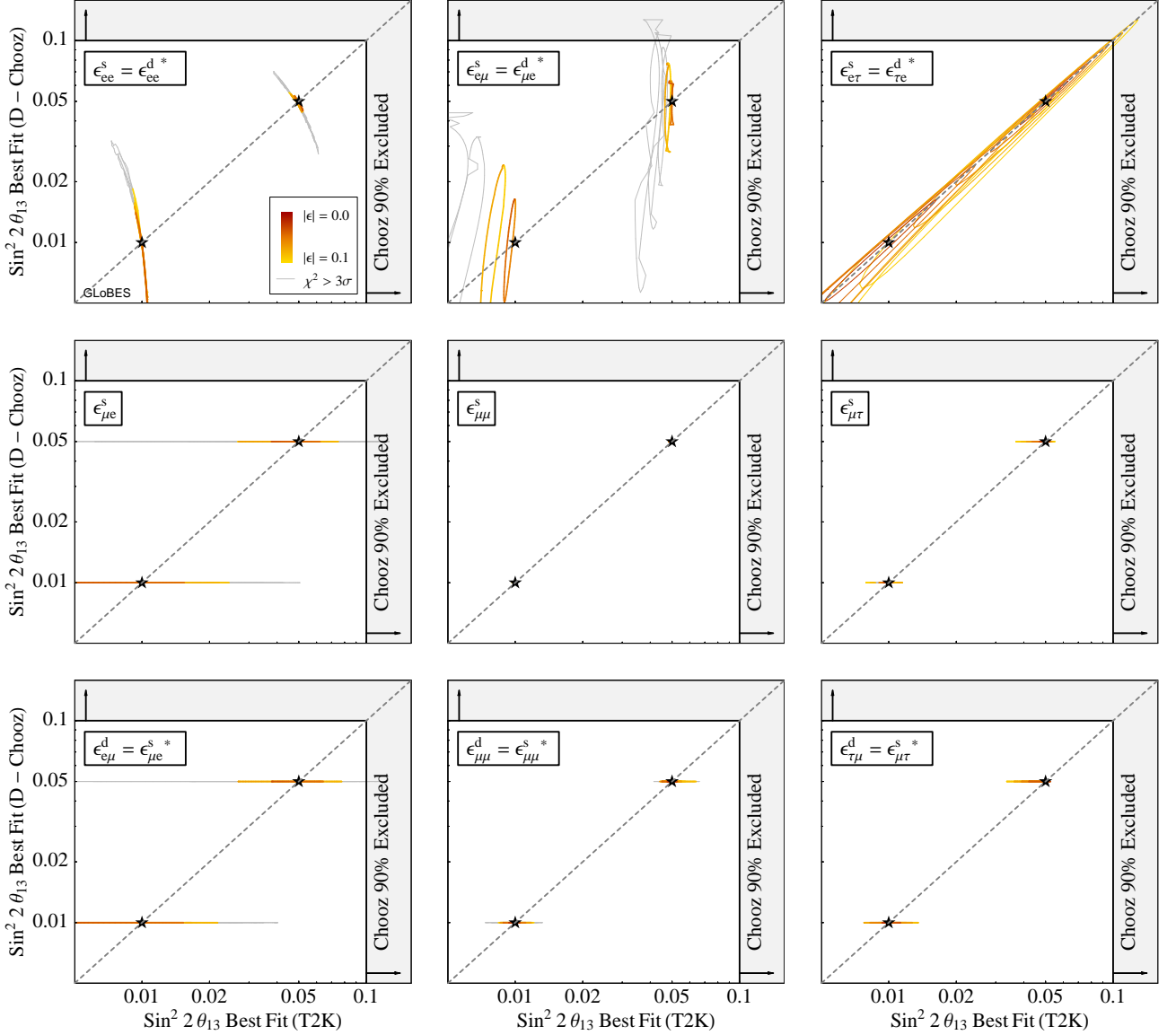


Figure 5: Distortion of the  $\theta_{13}$  fits in T2K and Double Chooz in the presence of  $\varepsilon_{\alpha\beta}^s$  and  $\varepsilon_{\beta\alpha}^d$ . For each plot, the modulus of the corresponding  $\varepsilon$  parameter has been varied from 0 to 0.1, and its phase from 0 to  $2\pi$ . For every such combination, we show the result of standard oscillation fits of  $\theta_{13}$ . Connected lines represent contours of equal  $|\varepsilon_{\alpha\beta}|$  and varying phase. Dark red (dark gray) lines correspond to  $|\varepsilon_{\alpha\beta}| = 0$ , while yellow (medium gray) lines correspond to  $|\varepsilon_{\alpha\beta}| = 0.1$ . Points giving a quality of fit worse than  $3\sigma$  in at least one of the two experiments are plotted in light gray. The black stars indicate the assumed “true”  $\sin^2 2\theta_{13}$ .

only create some tension, but no unambiguous contradiction between the beam and reactor fits.

Of the non-standard matter effects, we expect from Tab. II that only  $\varepsilon_{e\mu}^m$  and  $\varepsilon_{e\tau}^m$  should have any effect on the  $\theta_{13}$  fits.  $\varepsilon_{e\mu}^m$  is already strongly constrained from charged lepton flavor violation experiments [47], but  $\varepsilon_{e\tau}^m$  may still have a large impact. In fact, for extreme values of this parameter, there is even the possibility that NO $\nu$ A would erroneously report a  $\theta_{13}$  value above the Chooz bound.

Let us emphasize that, in order to obtain reliable estimates for the impact of non-standard interactions on reactor and superbeam experiments, it is crucial to take the information from the near detectors into account. To

show this, we have also studied how Figs. 5 and 6 get modified if we use a simplified simulation, in which the near detector does not appear explicitly, but only through suitably small values for the systematical uncertainties. In doing so, we have again treated  $\varepsilon^s$  and  $\varepsilon^d$  as completely independent matrices, possibly violating Eqs. (16) and (17). Thus, the results are also applicable to setups where  $\varepsilon^s$  and  $\varepsilon^d$  are indeed unrelated. In accordance with our expectations from Tab. II, we have found:

- For  $\varepsilon_{ee}^s$  and  $\varepsilon_{ee}^d$ , the effect on the reactor becomes stronger without the proper treatment of the near detector, because these terms no longer cancel then. Moreover, the discovery potential becomes worse,



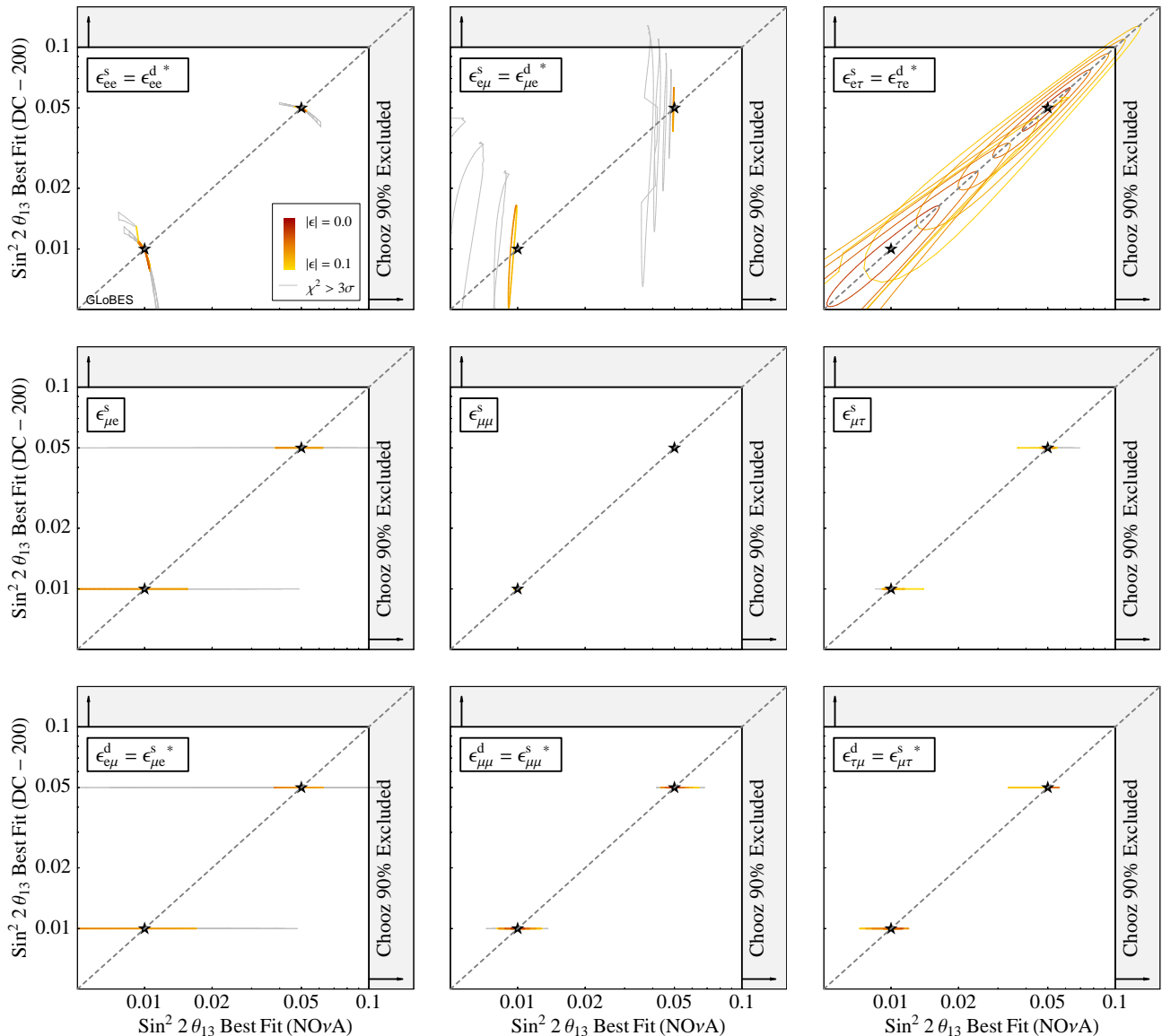


Figure 6: Effect of  $\varepsilon_{\alpha\beta}^s$  and  $\varepsilon_{\beta\alpha}^d$  on the  $\theta_{13}$  fits in NOvA and DC-200. The color-coding is the same as in Fig. 5.

i.e. there will be fewer gray segments in the plot.

- For the superbeam, the discovery of  $\varepsilon_{\mu e}^s$  and  $\varepsilon_{\mu e}^d$  becomes also much harder without the near detector, because the clear signature of an apparently modified  $\nu_e$  flux at the near site is no longer available. Moreover, for  $\varepsilon_{\mu e}^d$ , the strong impact of the NSI on the  $\theta_{13}$  fit in the superbeam, which we have identified as a near detector effect in the above discussion, vanishes in the single-detector simulation.
- The contours for  $\varepsilon_{e\tau}^s = \varepsilon_{\tau e}^{d*}$  are deformed without the near detector because in this (unrealistic) situation, it is no longer possible to misinterpret the non-standard effect as a reactor flux calibration error. Note that this misinterpretation is only due to the fact that  $\varepsilon_{e\tau}^s$  and  $\varepsilon_{\tau e}^{d*}$  are identical, since the

near detector is only affected if both are present (cf. Tab. II). Otherwise, it would retain its capability to properly calibrate the reactor flux to its true value.

So far, we have only considered situations in which one non-standard parameter is dominant, and all others are negligible. In realistic models, however, many parameters may be of the same order of magnitude. Since it is impossible to visualize the resulting high-dimensional parameter space, we resort to the scatter plots shown in Fig. 8. These plots were created by choosing a random value for each NSI parameter, and then performing a standard oscillation fit to the resulting experimental data. The moduli of the  $\varepsilon$  parameters were logarithmically distributed between  $10^{-8}$  and their current upper limits, where we have assumed the model-independent

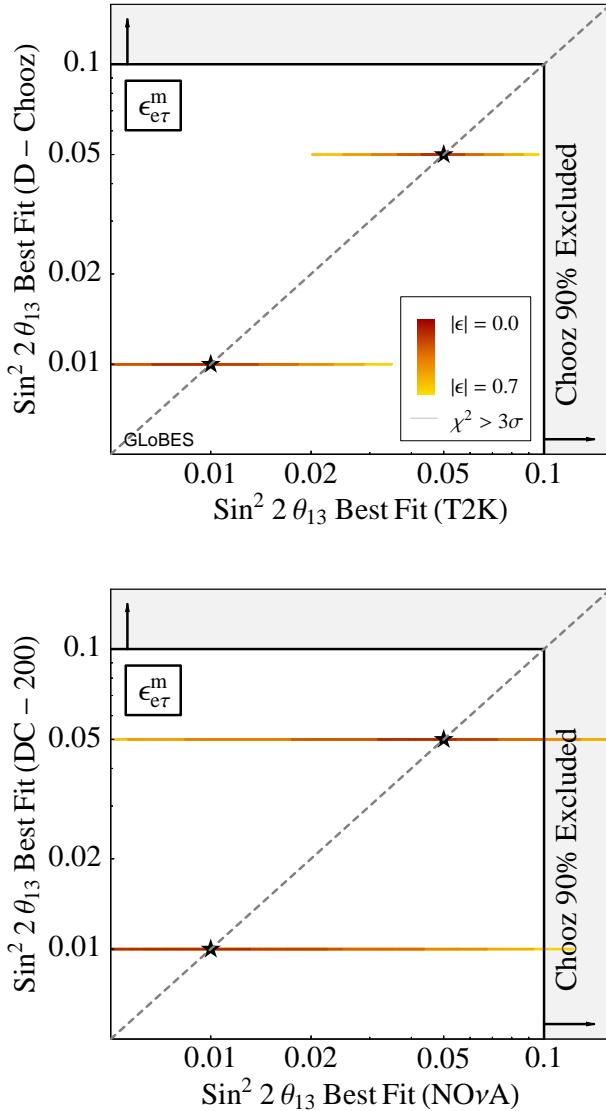


Figure 7: Effect of  $\varepsilon_{e\tau}^m$  on the  $\theta_{13}$  fits in T2K and Double Chooz, resp. in NO $\nu$ A and DC-200. We do not show plots for the other entries of  $\varepsilon^m$ , since these are either strongly constrained already ( $\varepsilon_{e\mu}^m$ ), or do not affect the  $\theta_{13}$  measurement ( $\varepsilon_{ee}^m$ ,  $\varepsilon_{\mu\mu}^m$ ,  $\varepsilon_{\mu\tau}^m$ , and  $\varepsilon_{\tau\tau}^m$ ). The color-coding is the same as in Fig. 5, but the scale is different since the bound on  $\varepsilon_{e\tau}^m$  is weaker than that for  $\varepsilon_{\alpha\beta}^{s,d}$  [31, 47].

bound from universality in charged lepton decays [31] for  $\varepsilon^s$  and  $\varepsilon^d$ , and the results of [47] for  $\varepsilon^m$ . The phases were distributed linearly between 0 and  $2\pi$ .

We can see from Fig. 8 that there are again points which yield a clear discrepancy in the  $\theta_{13}$  fits of the reactor and superbeam data, and others which correspond to a common offset of the fit value. The color coding shows that for a considerable fraction of the parameter space, the non-standard effect can actually be discovered. It is interesting to observe that there are some points for which the reactor fit lies above the Chooz bound. This

indicates that already with the present data, some parts of the parameter space could be ruled out.

## 6. DISCOVERY REACH FOR NON-STANDARD INTERACTIONS IN A COMBINED ANALYSIS OF REACTOR AND SUPERBEAM DATA

Let us now discuss the prospects of actually detecting the presence of non-standard interactions in reactor and superbeam experiments. We define the *discovery reach* as the range of  $\varepsilon$  parameters for which the quality of a standard oscillation fit is below a given confidence level. In Figs. 9 to 12, we show numerical results for this quantity, which were obtained by performing standard oscillation fits to the combined data of *both* experiments.

The results can again be interpreted with the help of Tab. II and of the formulas derived in Sec. 3. We see that for those non-standard parameters which have a large impact on any of the observed oscillation channels, there is typically also a good discovery potential. For some parameters, it comes from the reactor measurement, for others, it is dominated by the superbeam. It is remarkable, however, that in the case  $\varepsilon_{e\tau}^s = \varepsilon_{\tau e}^{d*}$ , there is practically no discovery potential at all, because neither experiment can discover these parameters on its own, and there is also no significant discrepancy between them, but only a common offset in their  $\theta_{13}$  fits.

It is interesting to observe that the good discovery reach for  $\varepsilon_{\mu\tau}^s$  comes from the *disappearance* channel, as can be easily verified from the corresponding analytical formulas in Sec. 3. Note that in those plots where  $\varepsilon_{\mu\tau}^s = \varepsilon_{\tau\mu}^{d*}$  is assumed, there is no discovery potential because the corresponding NSI terms in Eq. (34) cancel.

The discovery reach depends strongly on the phases of the NSI coupling constants,  $\phi_{\alpha\beta}^{s,d,m}$ . To first order in  $s_{13}$ , all off-diagonal entries of the  $\varepsilon$  matrices (except the  $\varepsilon_{\tau\mu}^s$  and  $\varepsilon_{\mu\tau}^d$  contributions in the  $\nu_\mu \rightarrow \nu_\mu$  disappearance channel) are accompanied by a combination of  $\phi_{\alpha\beta}^{s,d,m}$  and  $\delta_{CP}$ . To first order in  $\Delta m_{21}^2/\Delta m_{31}^2$ , they typically appear together with factors of  $\cos \phi_{\alpha\beta}^{s,d}$  or  $\sin \phi_{\alpha\beta}^{s,d}$ . The diagonal components of the  $\varepsilon$  matrices usually have prefactors of  $\cos \phi_{\alpha\alpha}^{s,d}$ .

The plots do not exhibit any phase dependence in the discovery reach for  $\varepsilon_{\mu e}^s$  and  $\varepsilon_{\mu e}^d$  because the sensitivity to these parameters comes mainly from the modified  $\nu_e$  flux in the near detector of the superbeam experiment. We have checked, that, in accordance with Eq. (30), the phase dependence would reappear if the near detector were omitted in the simulation.

Turning to non-standard matter effects described by  $\varepsilon^m$ , it is clear that the discovery potential will be very limited, since already standard matter effects are small in T2K and NO $\nu$ A, and completely negligible in Double Chooz and DC-200. Therefore, we use a different scale for the horizontal axis in Figs. 11 and 12. However, for some entries of  $\varepsilon^m$ , the present bounds are very weak.

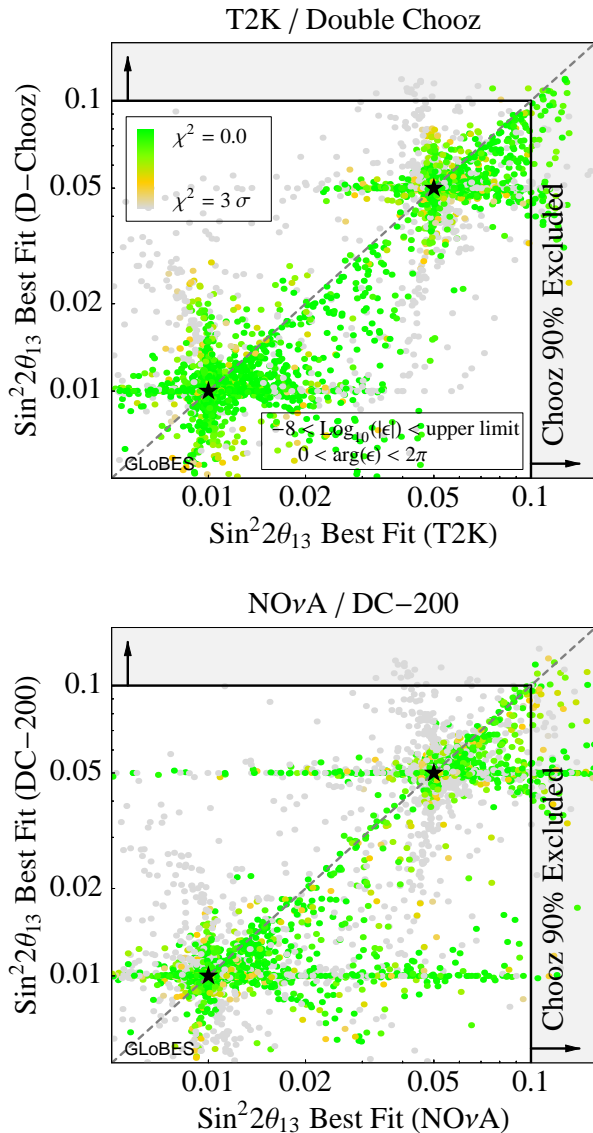


Figure 8: Possible outcomes of standard three-flavor oscillation fits to reactor and superbeam data in the presence of non-standard interactions. Each plot contains two datasets, one for  $\sin^2 2\theta_{13}^{\text{true}} = 0.01$ , and one for  $\sin^2 2\theta_{13}^{\text{true}} = 0.05$  (indicated by the black stars). For each dataset, 5,000 random combinations of  $\varepsilon$  parameters were chosen, with their moduli being distributed logarithmically between  $10^{-8}$  and the respective upper bounds [31, 47], and their phases varying linearly between 0 and  $2\pi$ . Each of these random non-standard scenarios was then fitted under the assumption of standard three-flavor oscillations. Green (dark gray) points indicate a very good quality of this fit, while light gray points denote a fit quality worse than  $3\sigma$  in at least one of the two experiments, i.e. an effective discovery of the non-standard effect. The plots show that non-standard interactions can induce ostensible discrepancies between reactor and superbeam data (off-diagonal points), or a common offset (close-to-diagonal points), which would lead to consistent, but wrong results. Note that some points lie even above the Chooz bound. A reactor fit above the Chooz bound indicates that the corresponding combination of NSI parameters and  $\theta_{13}^{\text{true}}$  could already be ruled out using existing data.

In particular we have  $\varepsilon_{ee}^m \lesssim 1.0$ ,  $\varepsilon_{e\tau}^m \lesssim 0.7$ , and  $\varepsilon_{\tau\tau}^m \lesssim 1.4$  [47]. Figs. 11 and 12 thus show that the bound on  $\varepsilon_{e\tau}^m$  could be improved by  $\text{NO}\nu\text{A}$ , but not by T2K. We should, however, keep in mind that, according to Eq. (7),  $|\varepsilon_{e\tau}^m| \sim 0.7$  corresponds to  $M_{\text{NSI}} \sim 100$  GeV, and it is hard to imagine a model, that could yield such a low NSI scale without violating present electroweak precision data. Both T2K and  $\text{NO}\nu\text{A}$  have some sensitivity also to  $\varepsilon_{e\mu}^m$  and  $\varepsilon_{\mu\tau}^m$ , but they cannot compete with the current bounds  $\varepsilon_{e\mu}^m \lesssim 5 \cdot 10^{-4}$  and  $\varepsilon_{\mu\tau}^m \lesssim 0.1$ .

Note that, according to Eqs. (33) and (35), the sensitivity to  $\varepsilon_{e\mu}^m$  and  $\varepsilon_{e\tau}^m$  comes from the  $\nu_e$  appearance channel, while the sensitivity to  $\varepsilon_{\mu\tau}^m$  has its origin in the disappearance channel.

Let us dwell for a moment on the interesting shape of the sensitivity contours for  $\varepsilon_{e\tau}^m$  and  $\varepsilon_{e\mu}^m$ , which can only be understood by taking into account terms proportional to  $|\varepsilon|^2$ . Let us consider, for example,  $\varepsilon_{e\mu}^m$ . According to Eq. (33), the NSI contribution to the oscillation probability is, to first order in  $|\varepsilon|$  and neglecting  $\Delta m_{21}^2$ ,

$$\begin{aligned}
& -4|\varepsilon_{e\mu}^m|s_{23}c_{23}^2\tilde{s}_{13}\cos(\phi_{e\mu}^m + \delta_{\text{CP}}) \\
& \cdot \left[ \sin^2 \frac{a_{\text{CC}}L}{4E} - \sin^2 \frac{\Delta m_{31}^2 L}{4E} + \sin^2 \frac{(\Delta m_{31}^2 - a_{\text{CC}})L}{4E} \right] \\
& -2|\varepsilon_{e\mu}^m|s_{23}c_{23}^2\tilde{s}_{13}\sin(\phi_{e\mu}^m + \delta_{\text{CP}}) \\
& \cdot \left[ \sin \frac{a_{\text{CC}}L}{2E} - \sin \frac{\Delta m_{31}^2 L}{2E} + \sin \frac{(\Delta m_{31}^2 - a_{\text{CC}})L}{2E} \right] \\
& + 8|\varepsilon_{e\mu}^m|s_{23}^3\tilde{s}_{13}\cos(\phi_{e\mu}^m + \delta_{\text{CP}})\frac{a_{\text{CC}}}{\Delta m_{31}^2 - a_{\text{CC}}} \\
& \cdot \sin^2 \frac{(\Delta m_{31}^2 - a_{\text{CC}})L}{4E}. \tag{38}
\end{aligned}$$

By carefully studying this expression, one finds that the energy dependence in the first and third terms of Eq. (38) is quite different from that of standard oscillations, which is proportional to  $\sin^2(\Delta m_{31}^2 - a_{\text{CC}})L/4E$ . Therefore, these terms will be easy to detect, while the second term, which modulates the spectrum in the same way as standard oscillations, can be absorbed into a modified  $\theta_{13}$  fit, and will therefore be hard to detect. From the phase dependence of these terms, we expect that, for our choice of  $\delta_{\text{CP}}^{\text{true}} = 0$ , the discovery reach should be good for  $\phi_{e\mu}^m \sim 0, \pi$ , and poor for  $\phi_{e\mu}^m \sim \frac{1}{2}\pi, \frac{3}{2}\pi$ . The plots in Figs. 11 and 12 reveal that the discovery reach indeed shows this behavior, except for an unexpectedly good sensitivity at  $\phi_{e\mu}^m = \frac{3}{2}\pi$ . To understand this, we have to take into account the second order terms, which we have found to be

$$\begin{aligned}
& 4|\varepsilon_{e\mu}^m|^2c_{23}^4\sin^2 \frac{a_{\text{CC}}L}{4E} \\
& + 4|\varepsilon_{e\mu}^m|^2s_{23}^4\left(\frac{a_{\text{CC}}}{\Delta m_{31}^2 - a_{\text{CC}}}\right)^2\sin^2 \frac{(\Delta m_{31}^2 - a_{\text{CC}})L}{4E} \\
& + 2|\varepsilon_{e\mu}^m|^2s_{23}^2\frac{a_{\text{CC}}}{\Delta m_{31}^2 - a_{\text{CC}}} \\
& \cdot \cos \frac{\Delta m_{31}^2 L}{4E}\sin \frac{a_{\text{CC}}L}{4E}\sin \frac{(\Delta m_{31}^2 - a_{\text{CC}})L}{4E}. \tag{39}
\end{aligned}$$

The important observation is that the net effect of the second order terms is always positive, while for the first order terms, it is positive at  $\phi_{e\mu}^m \simeq \frac{3}{2}\pi$ , and negative at  $\phi_{e\mu}^m \simeq \frac{1}{2}\pi$ . In the first case, we would therefore need a much stronger deviation of the fitted  $\theta_{13}$  from its true value in order to absorb the non-standard term. This, however, is disfavored by the reactor measurement, so that the combined fit improves the discovery reach by a considerable amount at  $\phi_{e\mu}^m \simeq \frac{3}{2}\pi$ . We are here in the interesting situation that the combination of seemingly redundant data sets can be beneficial if there are deviations from standard three-flavor oscillations. For most other non-standard parameters, the discovery reach is dominated by either the reactor or the superbeam.

## 7. CONCLUSIONS

In this paper, we have studied the impact of non-standard neutrino interactions on upcoming reactor and accelerator neutrino experiments. We have first classified the allowed NSI terms in the Lagrangian according to their Lorentz structure, and have found that many of them are irrelevant to reactor and superbeam setups. Those which can have an impact are mostly of the  $(V - A)(V \pm A)$  type, but in superbeam experiments, also  $(S + P)(S \pm P)$  type effects can be important. Since reactor and superbeam experiments are not able to distinguish different Lorentz structures, we have reparameterized the NSI coupling constants in order to greatly reduce the number of free parameters in the problem.

Using this reparameterization, we have then derived approximate analytic expressions for the non-standard neutrino oscillation probabilities, both in vacuum and in matter of constant density. We have developed an intuitive understanding of the terms relevant to specific oscillation channels, and have classified them accordingly.

In the second part of our work, we have performed detailed numerical simulations using GLOBES. We have considered two scenarios: T2K combined with Double Chooz, and NO $\nu$ A combined with a 200 t reactor experiment, dubbed DC-200. Our simulations take into account parameter correlations, degeneracies, and systematical errors, and in particular, we employ a realistic treatment of the near detectors. We have found that non-standard interactions can have a sizeable impact on future reactor and superbeam experiments, if the coupling constants are

close to their current upper limits, and if complex phases do not conspire to cancel them. The biggest impact is on the  $\theta_{13}$  measurement: If NSI are not properly taken into account in the fit, the results may be significantly wrong. There are scenarios in which a clear discrepancy between reactor and superbeam experiments shows up, but we can also have the situation that both fits seem to agree very well, but the derived  $\theta_{13}$  value has a significant offset from the true value. It is even possible that the true  $\theta_{13}$  is erroneously “ruled out” at  $3\sigma$ . To detect this kind of problems, a third experiment, complementary to the other two, would be required. Thus, we see that the possibility of non-standard effects should always be kept in mind when planning or analyzing upcoming experiments.

We have also studied the discovery potential for NSI in reactor and superbeam experiments, i.e. the range of non-standard parameters, which can actually be detected by these experiments because the quality of a standard oscillation fit becomes poor. We have found that, depending on the complex phases, some NSI may be discovered if their coupling constants are not more than a factor of 5 smaller than the current upper bounds. The best discovery reach is obtained only if both, reactor and superbeam experiments, and also the respective near detectors are considered in the analysis. In most cases, one of the experimental channels dominates the discovery reach, but there are also situations where only the discrepancy between the single-experiment fits indicates the presence of NSI. Our discussion thus shows that reactor and superbeam measurements, which might seem to be redundant in the standard three-flavor framework, turn out to be highly complementary once non-standard effects are considered.

## Acknowledgments

This work was in part supported by the Transregio Sonderforschungsbereich TR27 “Neutrinos and Beyond” der Deutschen Forschungsgemeinschaft. The work of JS is supported in part by the Grant-in-Aid for the Ministry of Education, Culture, Sports, Science, and Technology, Government of Japan (No. 17740131 and 18034001). JK would like to acknowledge support from the Studienstiftung des Deutschen Volkes.

- 
- [1] L. Wolfenstein, Phys. Rev. **D17**, 2369 (1978).  
 [2] J. W. F. Valle, Phys. Lett. **B199**, 432 (1987).  
 [3] M. M. Guzzo, A. Masiero, and S. T. Petcov, Phys. Lett. **B260**, 154 (1991).  
 [4] E. Roulet, Phys. Rev. **D44**, R935 (1991).  
 [5] S. Bergmann, Y. Grossman, and E. Nardi, Phys. Rev. **D60**, 093008 (1999), hep-ph/9903517.  
 [6] T. Hattori, T. Hasuike, and S. Wakaizumi, Prog. Theor. Phys. **114**, 439 (2005), hep-ph/0210138.  
 [7] M. Garbutt and B. H. J. McKellar (2003), hep-ph/0308111.  
 [8] M. Blennow, T. Ohlsson, and W. Winter, Eur. Phys. J. **C49**, 1023 (2007), hep-ph/0508175.  
 [9] A. De Gouvea, G. F. Giudice, A. Strumia, and K. Tobe, Nucl. Phys. **B623**, 395 (2002), hep-ph/0107156.  
 [10] T. Ota and J. Sato, Phys. Rev. **D71**, 096004 (2005), hep-

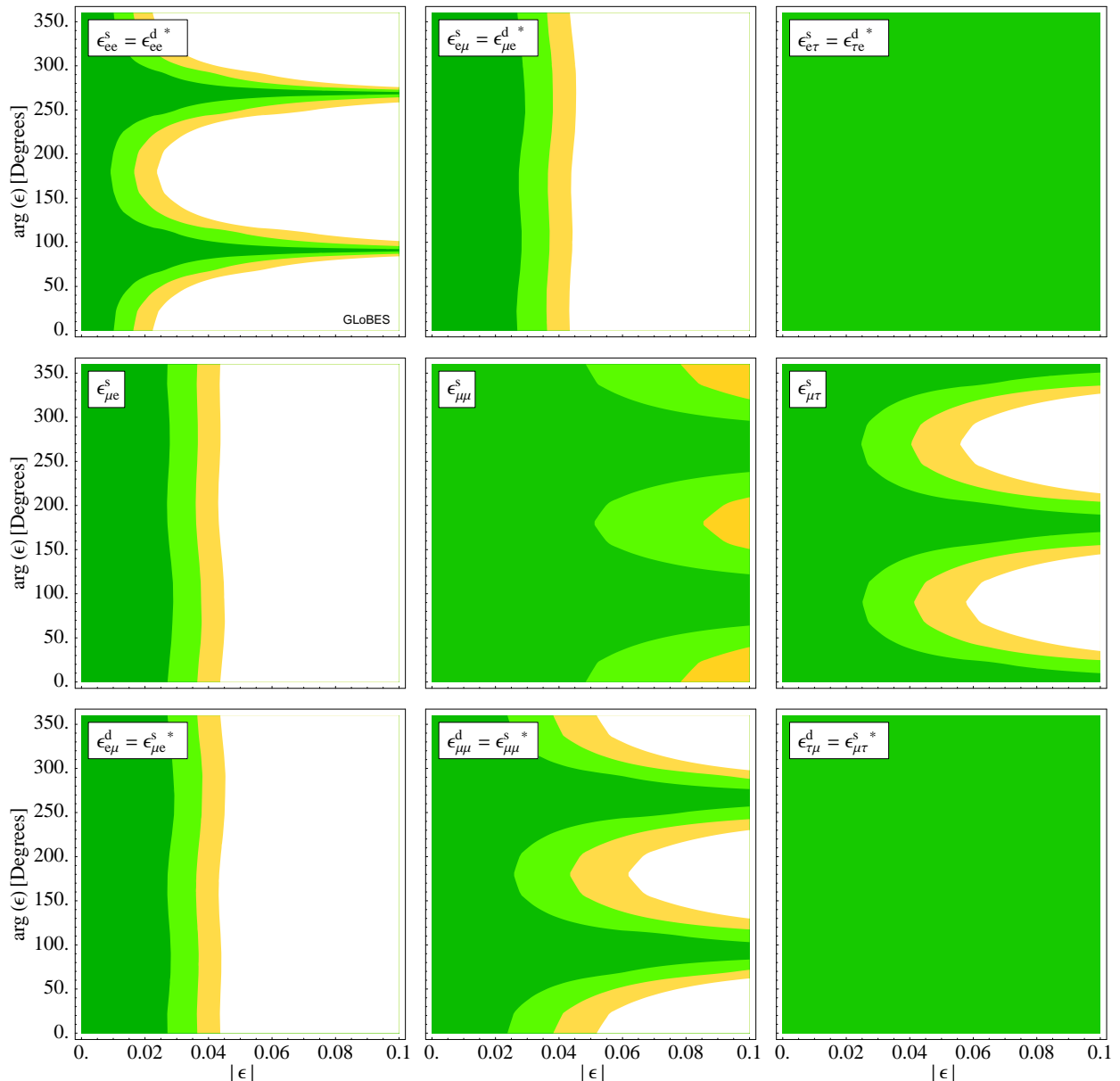


Figure 9: Discovery reach for  $\varepsilon_{\alpha\beta}^s$  and  $\varepsilon_{\beta\alpha}^d$  in a combined analysis of T2K and Double Chooz. Contours for  $1\sigma$ ,  $2\sigma$ , and  $3\sigma$  are shown. A true value of  $\sin^2 2\theta_{13}^{\text{true}} = 0.05$  was assumed, but we have checked that the results do not depend on  $\sin^2 2\theta_{13}^{\text{true}}$ .

- ph/0502124.
- [11] M. Honda, Y. Kao, N. Okamura, A. Pronin, and T. Takeuchi (0400), arXiv:0704.0369 [hep-ph].
- [12] M. Honda, Y. Kao, N. Okamura, A. Pronin, and T. Takeuchi (2007), arXiv:0707.4545 [hep-ph].
- [13] Y. Grossman, Phys. Lett. **B359**, 141 (1995), hep-ph/9507344.
- [14] S. Bergmann, M. M. Guzzo, P. C. de Holanda, P. I. Krastev, and H. Nunokawa, Phys. Rev. **D62**, 073001 (2000), hep-ph/0004049.
- [15] Z. Berezhiani, R. S. Raghavan, and A. Rossi, Nucl. Phys. **B638**, 62 (2002), hep-ph/0111138.
- [16] A. Friedland, C. Lunardini, and C. Pena-Garay, Phys. Lett. **B594**, 347 (2004), hep-ph/0402266.
- [17] O. G. Miranda, M. A. Tortola, and J. W. F. Valle, JHEP **10**, 008 (2006), hep-ph/0406280.
- [18] M. C. Gonzalez-Garcia et al., Phys. Rev. Lett. **82**, 3202 (1999), hep-ph/9809531.
- [19] S. Bergmann, Y. Grossman, and D. M. Pierce, Phys. Rev. **D61**, 053005 (2000), hep-ph/9909390.
- [20] N. Fornengo, M. Maltoni, R. T. Bayo, and J. W. F. Valle, Phys. Rev. **D65**, 013010 (2001), hep-ph/0108043.
- [21] M. C. Gonzalez-Garcia and M. Maltoni, Phys. Rev. **D70**, 033010 (2004), hep-ph/0404085.
- [22] A. Friedland, C. Lunardini, and M. Maltoni, Phys. Rev. **D70**, 111301 (2004), hep-ph/0408264.
- [23] A. Friedland and C. Lunardini, Phys. Rev. **D72**, 053009 (2005), hep-ph/0506143.
- [24] S. Bergmann and Y. Grossman, Phys. Rev. **D59**, 093005 (1999), hep-ph/9809524.

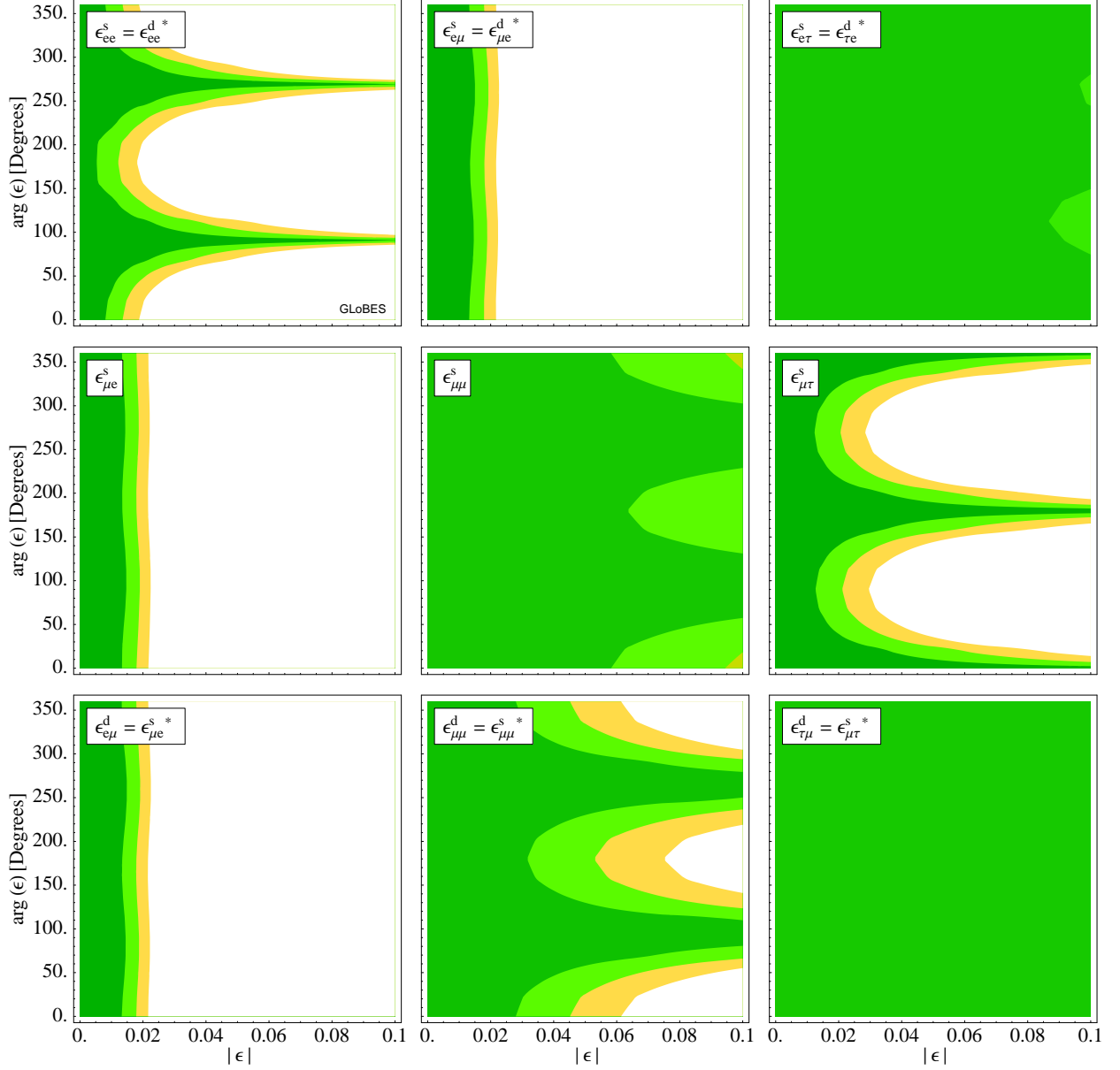


Figure 10: Discovery reach for  $\epsilon_{\alpha\beta}^s$  and  $\epsilon_{\beta\alpha}^d$  in a combined analysis of NO $\nu$ A and DC-200. Contours for  $1\sigma$ ,  $2\sigma$ , and  $3\sigma$  are shown. A value of  $\sin^2 2\theta_{13}^{\text{true}} = 0.05$  was assumed in the simulation, but we have checked that the results remain unchanged if we go to a different  $\sin^2 2\theta_{13}^{\text{true}}$ .

- [25] T. Ota, J. Sato, and N.-a. Yamashita, Phys. Rev. **D65**, 093015 (2002), hep-ph/0112329.
- [26] T. Ota and J. Sato, Phys. Lett. **B545**, 367 (2002), hep-ph/0202145.
- [27] M. Honda, N. Okamura, and T. Takeuchi (2006), hep-ph/0603268.
- [28] N. Kitazawa, H. Sugiyama, and O. Yasuda (2006), hep-ph/0606013.
- [29] A. Friedland and C. Lunardini, Phys. Rev. **D74**, 033012 (2006), hep-ph/0606101.
- [30] M. Blennow, T. Ohlsson, and J. Skrotzki (2007), hep-ph/0702059.
- [31] M. C. Gonzalez-Garcia, Y. Grossman, A. Gusso, and Y. Nir, Phys. Rev. **D64**, 096006 (2001), hep-ph/0105159.
- [32] P. Huber and J. W. F. Valle, Phys. Lett. **B523**, 151 (2001), hep-ph/0108193.
- [33] A. M. Gago, M. M. Guzzo, H. Nunokawa, W. J. C. Teves, and R. Zukanovich Funchal, Phys. Rev. **D64**, 073003 (2001), hep-ph/0105196.
- [34] P. Huber, T. Schwetz, and J. W. F. Valle, Phys. Rev. **D66**, 013006 (2002), hep-ph/0202048.
- [35] M. Campanelli and A. Romanino, Phys. Rev. **D66**, 113001 (2002), hep-ph/0207350.
- [36] A. Bueno, M. Campanelli, M. Laveder, J. Rico, and A. Rubbia, JHEP **06**, 032 (2001), hep-ph/0010308.
- [37] J. Kopp, M. Lindner, and T. Ota, Phys. Rev. **D76**, 013001 (2007), hep-ph/0702269.
- [38] R. Adhikari, S. K. Agarwalla, and A. Raychaudhuri,

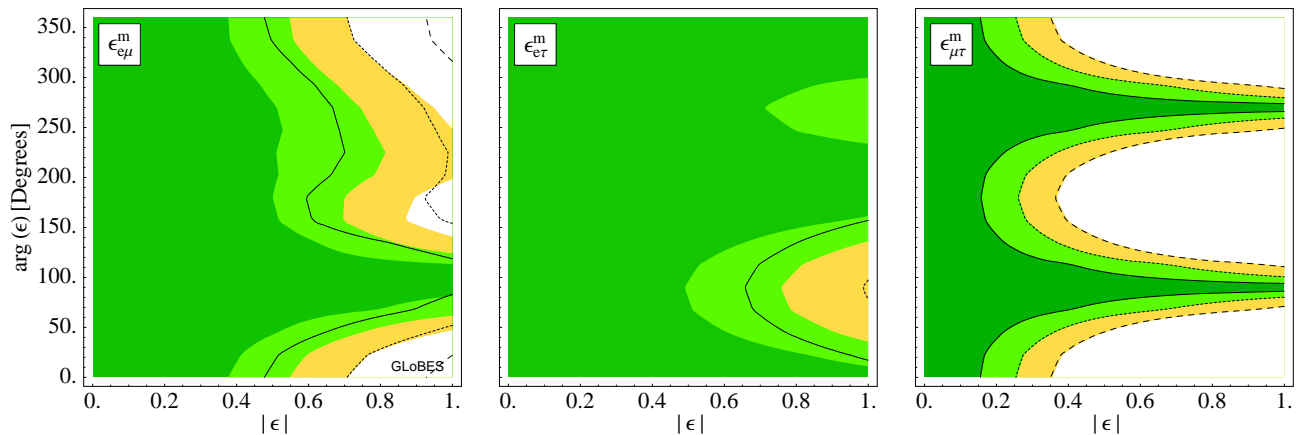


Figure 11: Discovery reach for  $\varepsilon_{\alpha\beta}^m$  in a combined analysis of T2K and Double Chooz. Since these experiments have essentially no sensitivity to  $\varepsilon_{ee}^m$ ,  $\varepsilon_{\mu\mu}^m$ , and  $\varepsilon_{\tau\tau}^m$ , we show only the off-diagonal entries of  $\varepsilon^m$ . The colored areas show the  $1\sigma$ ,  $2\sigma$ , and  $3\sigma$  confidence regions for  $\sin^2 2\theta_{13} = 0.05$ , while the black contours are for  $\sin^2 2\theta_{13} = 0.01$ . Note that the scaling of the horizontal axis is different from Figs. 9 and 10.

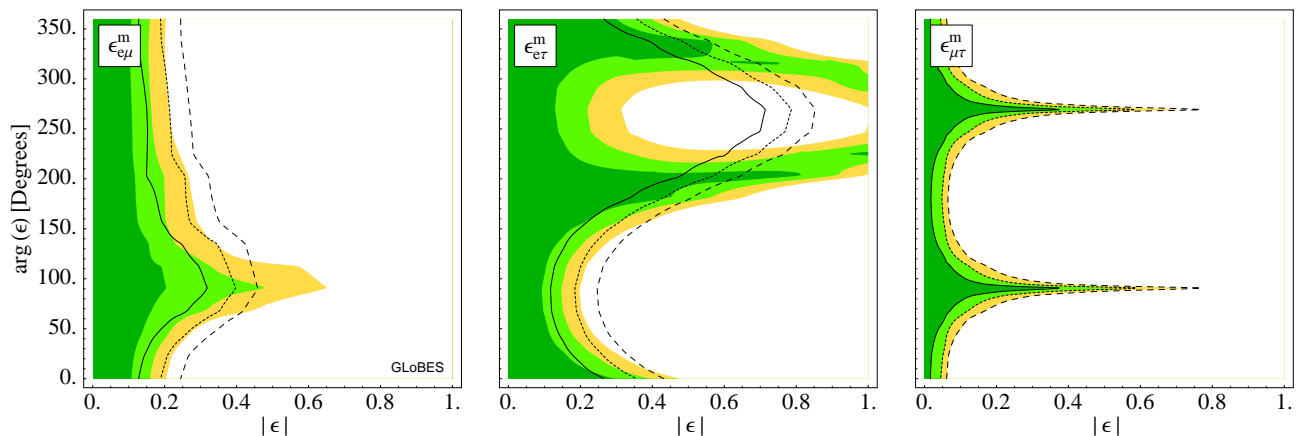


Figure 12: Discovery reach for  $\varepsilon_{\alpha\beta}^m$  in a combined analysis of NOνA and DC-200. Since these experiments have essentially no sensitivity to  $\varepsilon_{ee}^m$ ,  $\varepsilon_{\mu\mu}^m$ , and  $\varepsilon_{\tau\tau}^m$ , we show only the off-diagonal entries of  $\varepsilon^m$ . The colored areas show the  $1\sigma$ ,  $2\sigma$ , and  $3\sigma$  confidence regions for  $\sin^2 2\theta_{13} = 0.05$ , while the black contours are for  $\sin^2 2\theta_{13} = 0.01$ . Note that the scaling of the horizontal axis is different from Figs. 9 and 10.

- Phys. Lett. **B642**, 111 (2006), hep-ph/0608034.
- [39] G. L. Fogli, E. Lisi, A. Mirizzi, and D. Montanino, Phys. Rev. **D66**, 013009 (2002), hep-ph/0202269.
- [40] H. Duan, G. M. Fuller, J. Carlson, and Y.-Z. Qian, Phys. Rev. Lett. **97**, 241101 (2006), astro-ph/0608050.
- [41] A. Esteban-Pretel, R. Tomas, and J. W. F. Valle, Phys. Rev. **D76**, 053001 (2007), arXiv:0704.0032 [hep-ph].
- [42] G. Mangano et al., Nucl. Phys. **B756**, 100 (2006), hep-ph/0607267.
- [43] Z. Berezhiani and A. Rossi, Phys. Lett. **B535**, 207 (2002), hep-ph/0111137.
- [44] J. Barranco, O. G. Miranda, C. A. Moura, and J. W. F. Valle, Phys. Rev. **D73**, 113001 (2006), hep-ph/0512195.
- [45] J. Barranco, O. G. Miranda, and T. I. Rashba, JHEP **12**, 021 (2005), hep-ph/0508299.
- [46] J. Barranco, O. G. Miranda, and T. I. Rashba, Phys. Rev. **D76**, 073008 (2007), hep-ph/0702175.
- [47] S. Davidson, C. Pena-Garay, N. Rius, and A. Santamaria, JHEP **03**, 011 (2003), hep-ph/0302093.
- [48] Y. Itow et al. (2001), hep-ex/0106019.
- [49] K. Nishikawa et al. (T2K) (2006), URL [http://j-parc.jp/NuclPart/pac\\_0606/pdf/p11-Nishikawa.pdf](http://j-parc.jp/NuclPart/pac_0606/pdf/p11-Nishikawa.pdf).
- [50] D. S. Ayres et al. (NOνA) (2004), hep-ex/0503053.
- [51] F. Ardellier et al. (2004), hep-ex/0405032.
- [52] F. Ardellier et al. (Double Chooz) (2006), hep-ex/0606025.
- [53] P. Huber, J. Kopp, M. Lindner, M. Rolinec, and W. Winter, JHEP **05**, 072 (2006), hep-ph/0601266.
- [54] X. Guo et al. (Daya Bay) (2007), hep-ex/0701029.
- [55] P. Herczeg, Phys. Rev. **D52**, 3949 (1995).

- [56] A. I. Vainshtein, V. I. Zakharov, and M. A. Shifman, *JETP Lett.* **22**, 55 (1975).
- [57] W. Fetscher, *Phys. Lett.* **B140**, 117 (1984).
- [58] W. M. Yao et al. (Particle Data Group), *J. Phys.* **G33**, 1 (2006).
- [59] E. A. Paschos, L. Pasquali, and J. Y. Yu, *Nucl. Phys.* **B588**, 263 (2000), hep-ph/0005255.
- [60] E. A. Paschos and J. Y. Yu, *Phys. Rev.* **D65**, 033002 (2002), hep-ph/0107261.
- [61] T. D. Lee and C.-N. Yang, *Phys. Rev.* **104**, 254 (1956).
- [62] C. S. Wu, E. Ambler, R. W. Hayward, D. D. Hoppes, and R. P. Hudson, *Phys. Rev.* **105**, 1413 (1957).
- [63] R. P. Feynman and M. Gell-Mann, *Phys. Rev.* **109**, 193 (1958).
- [64] J. C. Hardy and I. S. Towner, *Phys. Rev. Lett.* **94**, 092502 (2005), nucl-th/0412050.
- [65] N. Severijns, M. Beck, and O. Naviliat-Cuncic, *Rev. Mod. Phys.* **78**, 991 (2006), nucl-ex/0605029.
- [66] E. K. Akhmedov, R. Johansson, M. Lindner, T. Ohlsson, and T. Schwetz, *JHEP* **04**, 078 (2004), hep-ph/0402175.
- [67] J. Arafune, M. Koike, and J. Sato, *Phys. Rev.* **D56**, 3093 (1997), hep-ph/9703351.
- [68] T. Ota and J. Sato, *Phys. Rev.* **D63**, 093004 (2001), hep-ph/0011234.
- [69] P. Huber, M. Lindner, and W. Winter, *Comput. Phys. Commun.* **167**, 195 (2005), hep-ph/0407333, URL <http://www.mpi-hd.mpg.de/~globes>.
- [70] P. Huber, J. Kopp, M. Lindner, M. Rolinec, and W. Winter, *Comput. Phys. Commun.* **177**, 432 (2007), hep-ph/0701187, URL <http://www.mpi-hd.mpg.de/~globes>.
- [71] P. Huber, M. Lindner, and W. Winter, *Nucl. Phys.* **B645**, 3 (2002), hep-ph/0204352.
- [72] M. Ishitsuka, T. Kajita, H. Minakata, and H. Nunokawa, *Phys. Rev.* **D72**, 033003 (2005), hep-ph/0504026.
- [73] M. D. Messier, Ph.D. thesis, Boston University (1999), UMI-99-23965.
- [74] P. Vogel and J. F. Beacom, *Phys. Rev.* **D60**, 053003 (1999), hep-ph/9903554.
- [75] T. Yang and S. Wojcicki (NOvA) (2004), Off-Axis-Note-SIM-30.
- [76] M. Maltoni, T. Schwetz, M. A. Tortola, and J. W. F. Valle, *New J. Phys.* **6**, 122 (2004), hep-ph/0405172.